



Bentonite Abandonment Plugs

Final Report Advanced Queensland Innovation Partnership (AQIP)
project

Celoxis System ID: 149354

Report release date: 30 April 2019



Research Team

Prof. Brian Towler, Dr. Heinz-Gerd Holl
School of Chemical Engineering, University of Queensland

Acknowledgements

This research was funded by The University of Queensland Centre for Coal Seam Gas (UQ-CCSG) and its industry members (Arrow Energy, Australia Pacific LNG and Santos – 2011 – 2021; and Shell (2011 - 2017)) and the Queensland Government Advance Queensland Innovation Partnerships program.

Citation

Holl, H. and Towler B. (2019). *Bentonite Abandonment Plugs: Final report Advance Queensland Innovation Partnership (AQIP) project*. The University of Queensland.
ISBN: 978-1-74272-358-7

Disclosure

The UQ, Centre of Coal Seam Gas is currently funded by the University of Queensland and the Industry members (Arrow Energy, Australia Pacific LNG, Santos). The Centre conducts research across Water, Geoscience, Petroleum Engineering and Social Performance themes.

For more information about the Centre's activities and governance see <http://www.ccsq.centre.uq.edu.au/>

Disclaimer

The information, opinions and views expressed in this report do not necessarily represent those of The University of Queensland, the Centre for Coal Seam Gas or its constituent members or associated companies. Researchers within or working with the Centre for Coal Seam Gas are bound by the same policies and procedures as other researchers within The University of Queensland, which are designed to ensure the integrity of research. You can view these policies at: <http://ppl.app.uq.edu.au/content/4.-research-and-research-training>

The Australian Code for the Responsible Conduct of Research outlines expectations and responsibilities of researchers to further ensure independent and rigorous investigations.

This report has not yet been independently peer reviewed.

Document Control Sheet

Version #	Reviewed by	Revision Date	Brief description of changes
1	Heinz Holl	15/03/2019	
1.1	Helen Schultz	21/03/2019	Initial review
1.2	Brian Towler	25/03/2019	Added an executive summary and minor editing
1.3	Helen Schultz	25/03/2019	Edited executive summary and included project overview
1.3	Andrew Garnett	26/03/2019	Added more to "industrial use" and commercialisation

Application of research findings in industry

The findings in this report indicate that bentonite is a viable method of sealing wells, whether they be coal seam gas wells, conventional oil and gas wells, water wells, or coal bores. The predominant focus of this project has been the detailed characterization, geomechanical testing and a field trial of bentonite plugs manufactured at UQ. In the final stages of the project preliminary tests to investigate a pumpable concept were also successfully undertaken.

Data previously published by Chevron indicate that plugging wells with bentonite is potentially cheaper and more reliable than plugging wells with a cement slurry. Consequently, this project is ripe for commercialisation.

Commercialisation is challenging. It will require investment in industrialised equipment for plug manufacture, supply agreements and for deployment equipment manufactured to oil field specifications. It may also demand that bentonite-cement hybrids be deployed in response to the conditions in a well. This makes equipment specification and service offering more complex.

Nevertheless, several routes to commercialisation have been or are being attempted. There are three major challenges:-

1. Generally speaking decommissioning or plugging and abandoning (P&A) is a form of “distress purchase”. Economically speaking it is almost always better to defer the expense and the operation rather than undertake it “now”. Therefore, it is difficult to secure a sufficiently large contract which would be needed to underpin investment in suitable oil field equipment required to industrialise the process. When there are P&A campaigns, they tend to be the more complex or urgent ones, a disincentive for trying a new technology.
2. The local industry has become adept at P&A operations making significant gains in operational efficiency and therefore cost reduction using convention cement technology. The cost-challenge for a new entrant has become harder.
3. Use of cement in P&A is a tried and trusted technology and is perceived as low risk. While UQ bentonite technology provides a hypothetically better sealing product, users may be loath to adopt it if this is perceived to cast doubt on the adequacy of the incumbent technology.

Executive Summary

The University of Queensland Centre for Coal Seam Gas (UQ CCSG) has investigated plugging wells with bentonite through laboratory experiments and with field trials. The first stage of this research was completed under the Centre-funded project: *Plugging CSG well with bentonite and other expansive clays*. The research was extended in this, the second project (AQIP project), funded by UQ CCSG and the Advance Queensland Innovation Partnership fund.

The bentonite used in the field trials and in the laboratory tests came from Amcol's mine north of Miles. Analysis of the bentonite in the three main seams at this mine was undertaken in the AQIP project and are provided in Table 2. Sibelco also operates a bentonite mine in the same area, but they did not provide bentonite for use in this study.

Laboratory tests have demonstrated that the 5D zone from Amcol's Gurulmundi mine produces the strongest plugs when hydrated, probably because that zone contains the most sodium montmorillonite, which we postulate has the best swelling behaviour. The 5A and 5B zone from the same mine were also tested and both of these are capable of sealing wells, but the plugs are not as strong as those manufactured with bentonite from the 5D zone.

The plugs were primarily tested on a specially built testing facility at The University of Queensland, consisting of 1 metre pipe sections of internal diameter 4", 6" and 8". These were stacked and flanged to each other to create taller test sections. However, plugs were also tested using a load frame shear cell. All of the plugs were manufactured using a specially built hydraulic press. The bentonite was combined with water and 1% poly vinyl pyridine (PVP) which acted as a binder to allow the bentonite to be pressed into a cylindrical shape suitable for dropping into a vertical well. The laboratory results showed that the 1% PVP actually makes the hydrated bentonite plug stronger.

Two field trials are discussed in this report. The first was on a water well (Bellevue 3) in the Bellevue CSG field, which was conducted in the previous UQ CCSG funded project, but is reported here for ease of reference. The second trial, which was undertaken in the AQIP project, was a coal bore on Greenswamp Rd, SW of Chinchilla. The Greenswamp Rd field trial tested the use of the bentonite plugs in combination with a shrinking compensated grout developed by Nautec Australia. Both wells were successfully sealed with bentonite plugs. A third field trial of a water well is under discussion with Arrow and may proceed after the conclusion of the AQIP project.

Preliminary tests to demonstrate the potential to develop a hybrid, pumpable bentonite product were also undertaken in the final phase of the AQIP project. In these laboratory experiments shrinking compensated grout (provided by Nautec Australia) was used to lubricate i) uncoated bentonite tablets (CETCO[®] tablets) and ii) 2" diameter 5D PVP bentonite plugs, which were pumped through hoses under pressure. Results indicate that a pumpable bentonite-based abandonment solution can be developed.

Table of Contents

Contents

1	Project Overview.....	6
2	Inventory of main bentonite deposits in Queensland and laboratory testing	6
2.1	Inventory based on DNRME database	7
2.2	Properties of tested bentonites.....	8
2.2.1	Mineralogy.....	8
2.2.2	Geochemistry.....	13
2.2.3	Mechanical properties testing	18
2.2.4	Small and Ultra Small Angle Neutron Scattering (SANS and USANS)	20
3	Failure mode and bentonite performance modelling (by Brian Towler, CCSG)	21
4	Ranking of the bentonite material based on mechanical dislodgment pressures	27
4.1	Hydraulic press tests.....	28
4.2	Load frame tests	30
5	First hydraulic tests using the Well Simulator Facility	32
6	Hydraulic long-term testing of the most promising materials	37
6.1	Results of the 4” pipe sections	37
6.2	Results of the 6” pipe sections	39
6.3	Results of the 8” pipe sections	40
6.4	Simulation of testing of bentonite plugs in uncased holes.....	41
6.5	Summary of the results of the hydraulic long term testing.....	45
7	“Pumpable solution”	47
8	Field trials.....	50
8.1	Bellevue #GW3 (Shell/QGC).....	50
8.2	Coal exploration well R 2315 (DNRME)	51
8.2.1	DNRME methane surveys	52
8.2.2	UQ Greenswamp Road coalhole and atmospheric methane surveys (by Dr Des Owen, CCSG) 52	
8.3	Water well RN 17414 (Arrow Energy).....	62
9	Grant applications for future development.....	62
10	Conclusions and outlook.....	62
11	References	65
12	Appendices	68

1 Project Overview

This project was funded by the UQ Centre for Coal Seam Gas and an Advance Queensland Innovation Partnership award. The project aimed to develop a novel, more reliable, lower cost plugging and abandonment (P&A) technology for the coal seam gas (CSG) industry. It built on a previous Centre-funded project that had successfully trialed the bentonite plug technology in a water monitoring bore (Bellevue #GW3 - Shell/QGC).

The laboratory program aimed to fully characterize the bentonite, undertake detailed technical assessments of plug performance under different sub-surface conditions, and provide the technical evidence to support the use of plugs in ‘non-ideal’ conditions e.g., uncased bores and wells. The project included a field trial of the bentonite technology in a coal exploration bore where high levels of methane emissions had been recorded. The field trial was conducted in collaboration with Department of Natural Resources, Mines & Energy, Renviro and Nautec Australia.

2 Inventory of main bentonite deposits in Queensland and laboratory testing

We used the summary of major mineral resources, mines and projects, published by the Department of Natural Resources and Mines, Queensland (von Gnielinski, 2017) to choose bentonite providers for the materials used in this project. Queensland is the biggest bentonite producing state in Australia. Bentonite is mined from large open cut deposits in the State’s southeast (Figure 1).

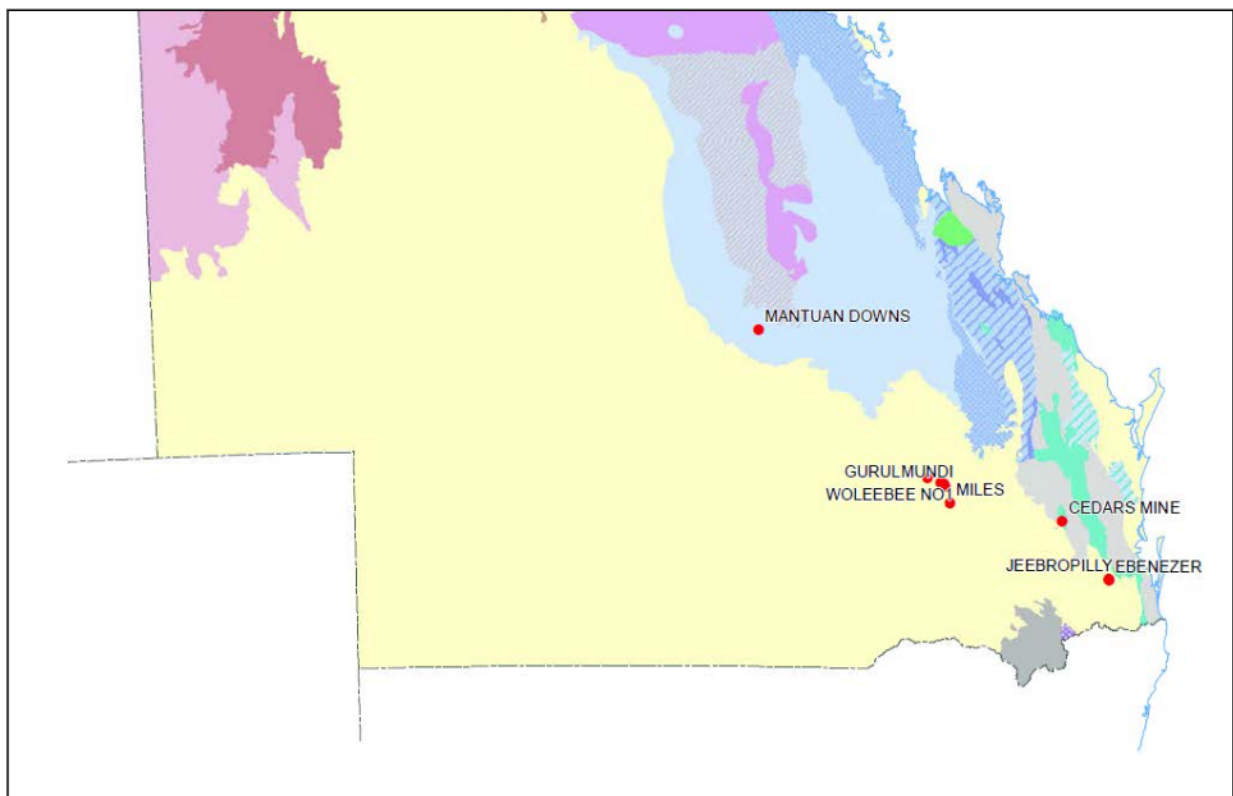


Figure 1: Bentonite deposits (red dots) in SE Queensland (von Gnielinski, 2017).

2.1 Inventory based on DNRME database

A summary of significant bentonite deposits in Queensland is given in Table 1.

Name	Location	Company
Cedars Mine	10km SW of Yarraman	PCP Douglass Pty Ltd
Ebenezer (Na bentonite)	10km SE of Ipswich	Clay Resources Company, a subsidiary of Ebenezer Mining Company Pty Ltd
Gurulmundi and Gurulmundi North (Na bentonite)	Gurulmundi township, 30km north of Miles	Sibelco
Jeebropilly Bentonite (Ca-Mg bentonite)	7 km SW of Ipswich	Jeebropilly Collieries Pty Ltd
Mantuan Downs	135km SW of Emerald	Pacific Enviromin Ltd
Miles (Na bentonite)	5km SW of Miles	Bioclay Pty Ltd trading as Miles Bentonite
Queensland Bentonite (high swelling Na bentonite)	36km NW of Miles and 6km W of Gurulmundi	Volclay International Ltd, operated by Amcol Australia Pty Ltd
Woleebee No. 1 (Na bentonite)	28.9km SW of Wandoan	Sibelco

Table 1: Summary of significant bentonite deposits in Queensland (after Gnielinski, 2017).

The largest sodium bentonite resources are located in the Miles-Gurulmundi region of the Darling Downs, some 300km WNW of Brisbane. The mined deposits are hosted by the Orallo Formation of the Jurassic/Cretaceous Surat Basin. The Orallo Formation comprises lithic sandstones, siltstones, minor mudstones and lenticular, bedded bentonite deposits near the top of the formation. The sediments are deposited in a fluvial/lacustrine to coastal plain/shallow marine environment (Scogings, 2014). The bentonite beds are overlain by laterally discontinuous conglomeratic channels at the bottom of the Lower Cretaceous, fluvial Mooga Sandstone. Scogings (2014) reported up to 10 different bentonite beds drilled at the area of the Queensland Bentonite Mine with a maximum layer thickness of up to 4m.

Sibelco Australia Pty Ltd is mining bentonite at the Woleebee No.1, the Gurulmundi, and Gurulmundi North mines and is Australia's largest bentonite producer (von Gnielinski, 2017). Amcol Australia Pty Ltd operates the nearby Queensland Bentonite Mine, producing high swelling sodium bentonite. All other providers mentioned in Table 1 are significantly smaller and are reporting less production. They also provide calcium and calcium-magnesium bentonites, which are less favorable for plug production because of slightly lower swelling performance.

We contacted Sibelco Australia Pty Ltd and Amcol Australia Pty Ltd to purchase the raw sodium bentonite material we used in our laboratory experiments and for the production of bentonite plugs for the commenced field trials.

Sibelco Pty Ltd decided not to provide raw samples for the proposed analytical program. It was not feasible to purchase supply from Sibelco Pty Ltd as the minimum purchase is 10 tonnes of processed ("activated") material, rather than the small amounts of raw material needed for our experimental purposes. We contacted DNRME Mineral Geoscience Section (March 2018) and requested their assistance in gaining samples from Sibelco Pty Ltd, however this has been unsuccessful.

Amcol Australia Pty Ltd provided the project with three different raw bentonite materials of their major deposits. These slightly different sodium bentonites were analyzed to determine the mineralogical composition and chemistry of the raw bentonite, swelling performance and mechanical properties to choose the best performing bentonite for the later abandonment field trials. QA/QC of

the bentonite used for the plug production was necessary to fulfill high quality standards used by the industry partners of the Centre for Coal Seam Gas at The University of Queensland (UQ CCSG).

The comparison of the technical data sheets of the bentonites of both providers showed little variations in chemistry, Cation Exchange Capacity (CEC), moisture content and bulk density. All Queensland commercial bentonite deposits are located in the same region and exhibit the same stratigraphic age/geological environment. They are all sodium-dominated bentonites and used for a range of agricultural, civil and geotechnical applications. The similarity of the commercially available bentonite indicates that large volumes of these resources with consistent chemical composition are available. No alternate commercially available source of the raw material could be identified from the information provided by the Geological Survey of Queensland. Consequently testing of additional bentonite resources was not required.

2.2 Properties of tested bentonites

2.2.1 Mineralogy

2.2.1.1 Mineralogical variations of three tested bentonite deposits

Amcol Australia Pty Ltd provided samples of the mined 5A, 5B and 5D bentonite seams. These three different raw bentonite materials of the major deposits in the Queensland Bentonite Mine were prepared for XRD measurements. The XRD analysis was conducted at the Central Analytic Research Facility (CARF) at QUT. Sample preparation and XRD measurement parameters and quantitative phase analysis methods are reported in detail by Raftery (2018) and Spratt & Raftery (2016a, 2016b). Graphics of the collected diffraction patterns along with the mineral phases identified are included at the end of their reports (see Appendix 01, 02 and 03). Three samples of each deposit were analyzed.

Table 2 and Figure 2 show the results of the quantitative phase analysis for the nine samples

	5D-1	5D-2	5D-3	5B-1	5B-2	5B-3	5A-1	5A-2	5A-3
Quartz	13.4	13.3	13.1	4.6	3.6	3.9	14.8	14.8	14.8
Albite	5.6	5.7	5.9	8.4	6.4	7.8	10.5	10.3	10.7
Anorthite	5.9	5.5	5.9	-	-	-	5.5	6.0	5.7
Smectite (Montmorillonite)	73.5	72.8	73.5	56.0	60.9	57.7	67.6	67.2	67.1
Zeolite	1.6	2.7	1.6	12.4	11.6	12.4	1.6	1.7	1.7
Opal (Cristobalite)	-	-	-	17.7	16.7	17.4	-	-	-
Gypsum	-	-	-	0.9	0.8	0.8	-	-	-

Table 2: Phase concentrations of the tested raw samples (nominal wt%, absolute). Each material was sampled and analyzed three times.

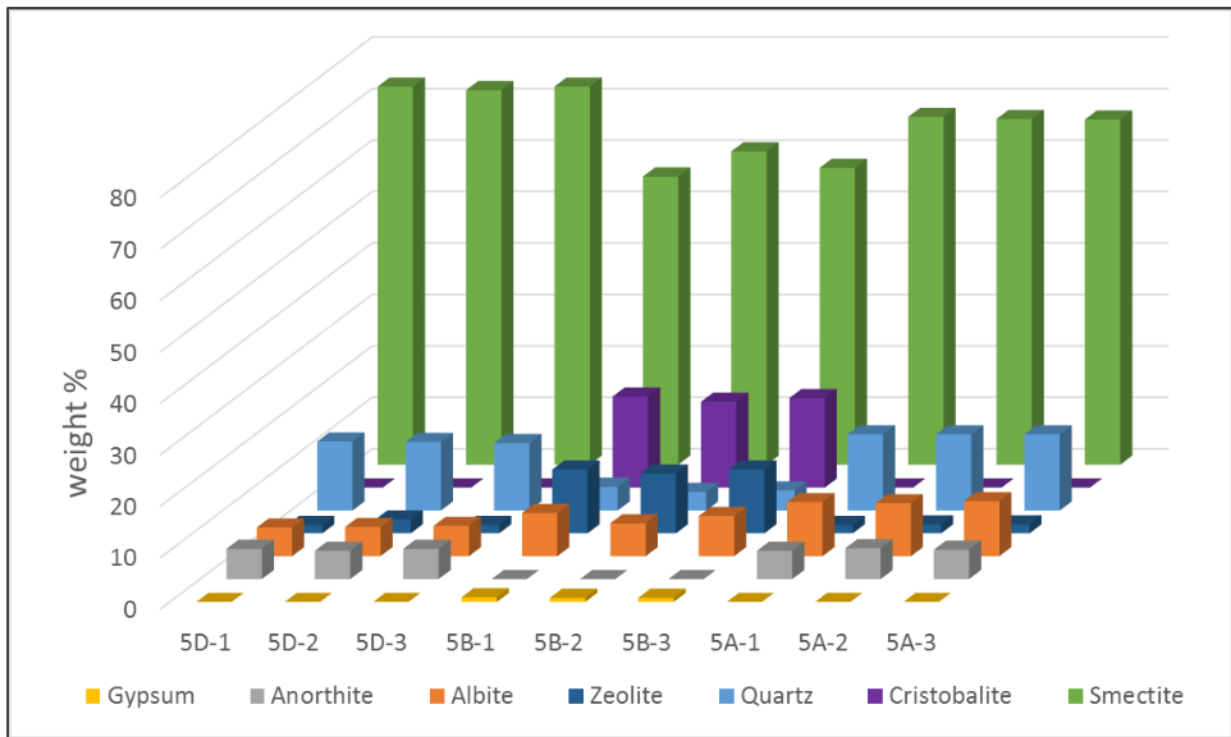


Figure 2: Bulk mineralogy of the tested samples.

It is clearly shown that the 5B bentonite deposit exhibits a different mineralogical composition compared to the 5D and 5A samples. The higher Cristobalite and Zeolite concentrations are causing a relative decrease of the absolute weight percentage of the montmorillonite in the bentonite, which has an impact on its Cation Exchange Capacity (CEC) and the swelling properties. The 5B bentonite is also the only tested material containing small amounts of gypsum (compare Scogings 2014).

Table 3 and Figure 3 are presenting the results of the analysis of the separated $<2\mu\text{m}$ fraction of the three bentonite samples.

	5D-1	5D-2	5D-3	5B-1	5B-2	5B-3	5A-1	5A-2	5A-3
Quartz	9.8	8.8	8.0	1.1	0.9	0.9	2.6	2.6	4.0
Albite	1.8	1.8	1.7	3.7	0.9	0.9	-	-	-
Smectite (Montmorillonite)	87.2	88.8	89.5	77.6	80.9	80.4	97.4	97.4	96.0
Zeolite	0.2	0.1	0.1	3.5	2.7	2.5	-	-	-
Opal (Cristobalite)	-	-	-	13.6	14.2	14.9	-	-	-
Kaolinite	0.9	0.6	0.6	-	-	-	-	-	-
Gypsum	-	-	-	0.5	0.4	0.4	-	-	-

Table 3: Phase concentrations of the $<2\mu\text{m}$ fraction (nominal wt%, absolute).

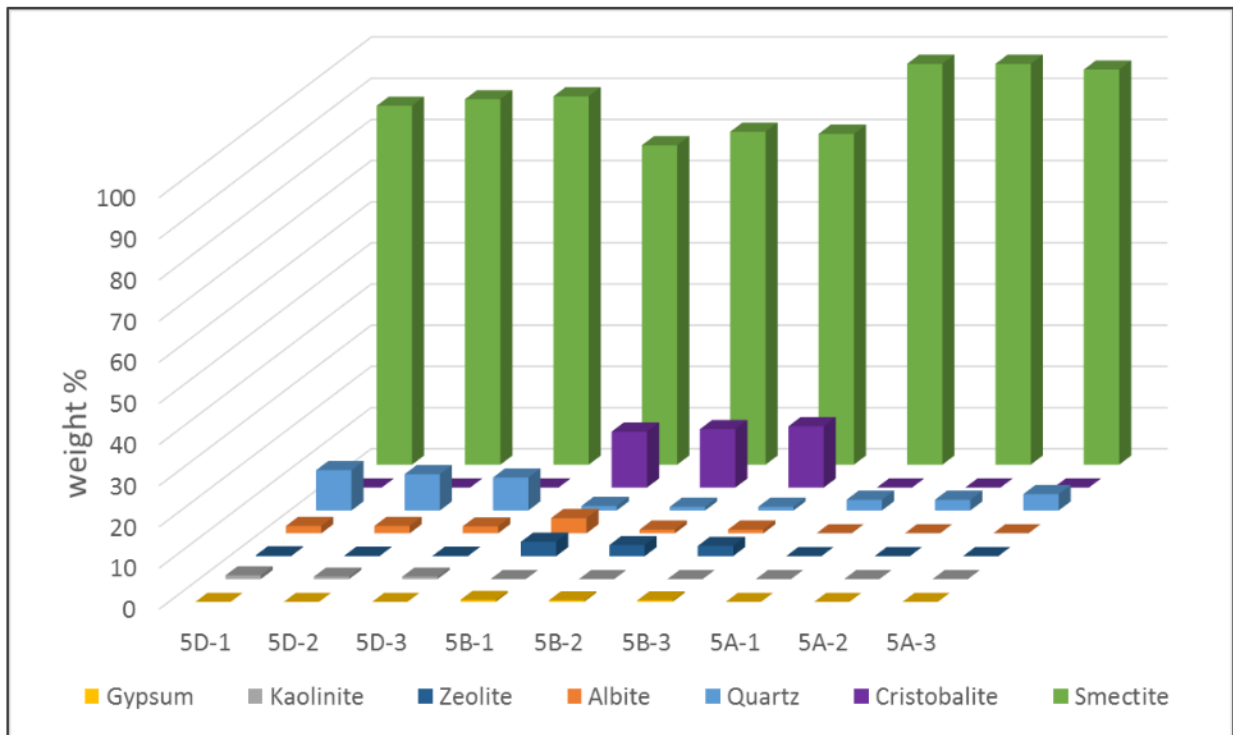


Figure 3: Bulk mineralogy of the analyzed <2μm fraction.

The clay fractions show similar results as the bulk mineralogy of the three sampled bentonites. The montmorillonite content in all samples of the <2μm fraction is higher than in the bulk material because of the enrichment of the clay particles in this grain size fraction. The difference between the tested bentonites is still evident: higher cristobalite and zeolite concentrations are affecting a relative decrease of the absolute weight percentage of the montmorillonite in the 5D material.

2.2.1.2 Quality assurance of the 5D bentonite used for plug manufacture

Figure 4 shows a comparison of all powder diffraction measurements and delineates the consistent bulk mineralogy of the material out of 7 bulk bags (three samples/bag) which was used to produce the plugs for both abandonment field trials in Queensland.

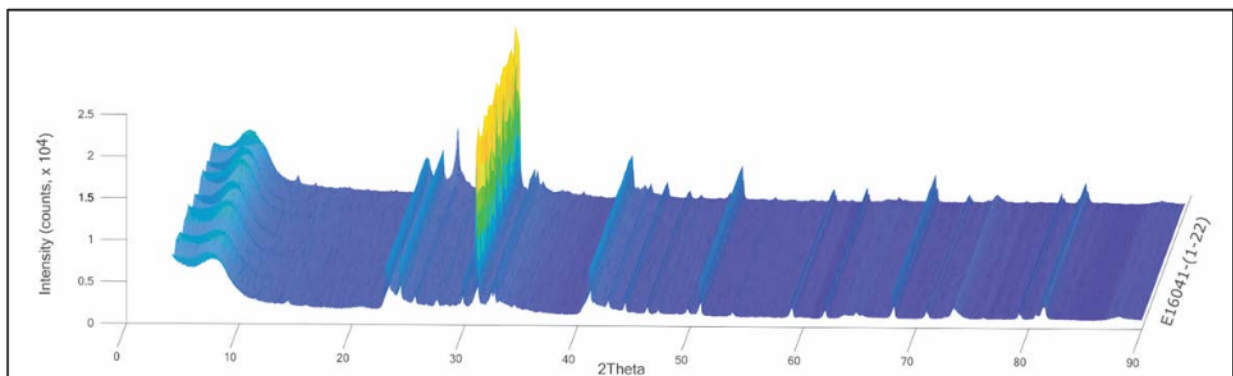


Figure 4: Comparison of powder XRD patterns of all analyzed samples.

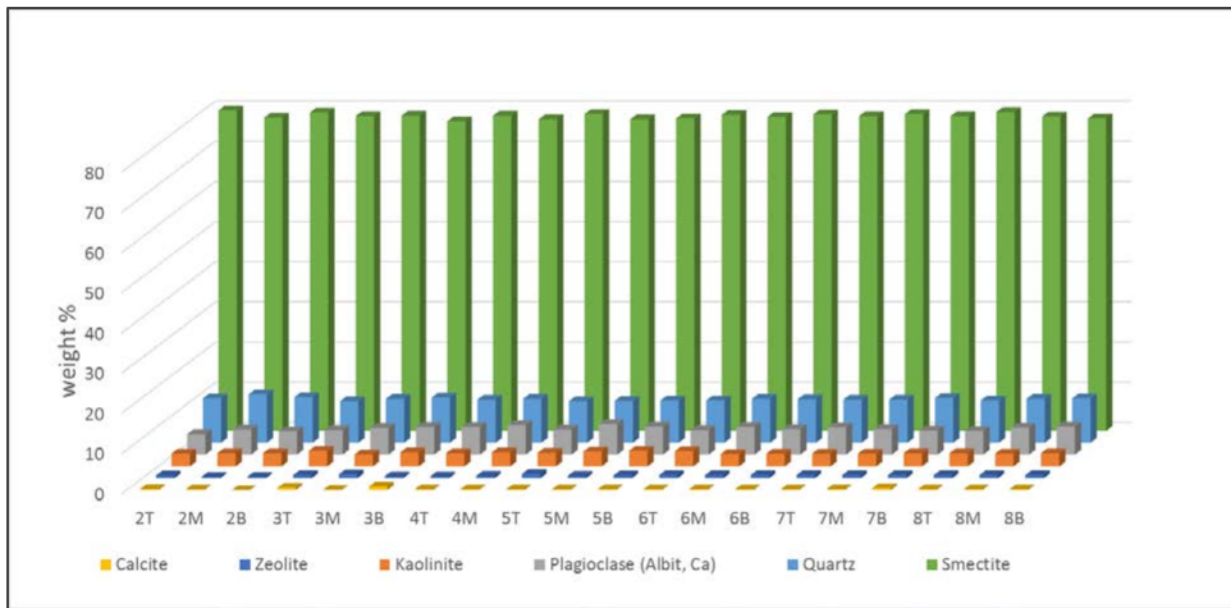


Figure 5: Bulk mineralogical composition of raw bentonite samples from 7 bulker bags of the Queensland Bentonite Mine 5D deposit. Each bag was sampled three times (Top/Middle/Bottom).

Figure 5 summarizes the results of the mineral quantification of the raw bentonite material. The identified mineral phases coincide with results published by Scogings (2014). He reported the occurrence of mainly dioctahedral smectite (montmorillonite) and lesser quantities of feldspar, kaolinite, quartz and zeolite varying in the different bentonite beds mined in Gurulmundi. The XRD measurements confirm the existence of montmorillonite, quartz and traces of kaolinite. Traces of calcite and clinoptilolite, a zeolite mineral, were also identified. The average bulk mineralogical composition of the raw bentonite is shown in Table 4.

Mineral content	Average wt % $\pm 2\sigma$
Quartz	10.8 ± 0.8
Kaolinite	3.4 ± 0.5
Plagioclase (Albite, Ca)	6.5 ± 1.1
Calcite	0.3 ± 0.4
Zeolite	0.7 ± 0.3
Smectite	78.3 ± 1.3

Table 4: Average bulk mineralogical composition (weight %) of raw bentonite samples from the Queensland bentonite Mine 5D deposit.

The clay mineralogy of the raw bentonite was determined using oriented clay specimens of the $<2\mu\text{m}$ fraction of the raw material. An example for a clay diffraction patterns (oriented specimens $<2\mu\text{m}$) is shown in Figure 6. The samples were measured air-dried, after being treated with ethylene glycol and after heating up to 375°C . This is a standard procedure in clay mineralogical determinations to characterize swelling clay minerals (Moore & Reynolds, 1997).

The position of the 001 reflections of the montmorillonite of the air-dried sample (dark blue curve in Figure 6) can be used to estimate the interlayer cation composition and the hydration state of the clay mineral (e.g. Oueslati et al., 2009). Treating the samples with ethylene glycol will produce very strong 001 peaks at lower 2 Theta angles (shifted to the left in Figure 6, green curve). These 001 peaks are sharp and symmetrical and show no low-angle shoulder, proving that no interstratified illite is present. Additionally the sample was heated to 375°C and measured again. The montmorillonite 001 peak collapses to higher 2 Theta angles (shifted to the right in Figure 6, red curve) and is losing intensity

(Moore & Reynolds, 1997).

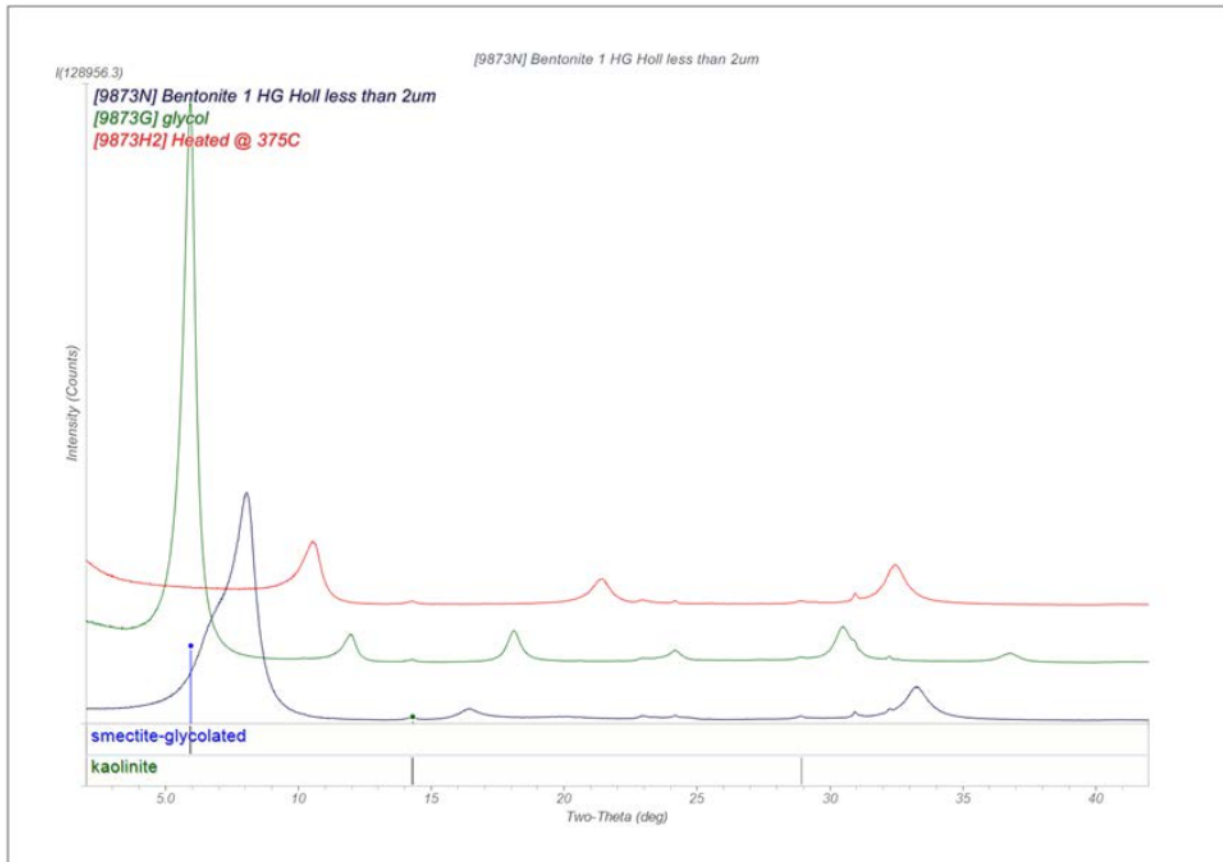


Figure 6: Clay XRD pattern, oriented specimen, <2µm.

The 001 reflections of the montmorillonite in the air-dried samples show asymmetric shoulders (Figure 6, blue curve and Figure 7). The peak doublets were fitted to model position and intensity of the distinct peaks. The 001 peaks of the <2µm fraction (Figure 7) are asymmetric with top at 8.1° 2Theta (d= 12.7 Å) and a shoulder on the low angle, high d-value side (6.8° 2Theta, d= 15.1 Å). D-values of 001 peaks of pure Na-montmorillonites with one layer of water molecules in the interlayer are usually close to 8.6° 2Theta (12 Å). The d-values of montmorillonites with divalent cations (Ca²⁺, Mg²⁺ etc.) and two layers of water molecules in the interlayer position are in range of 7.3-6.8° 2Theta (14-15 Å) (Carlson, 2004).

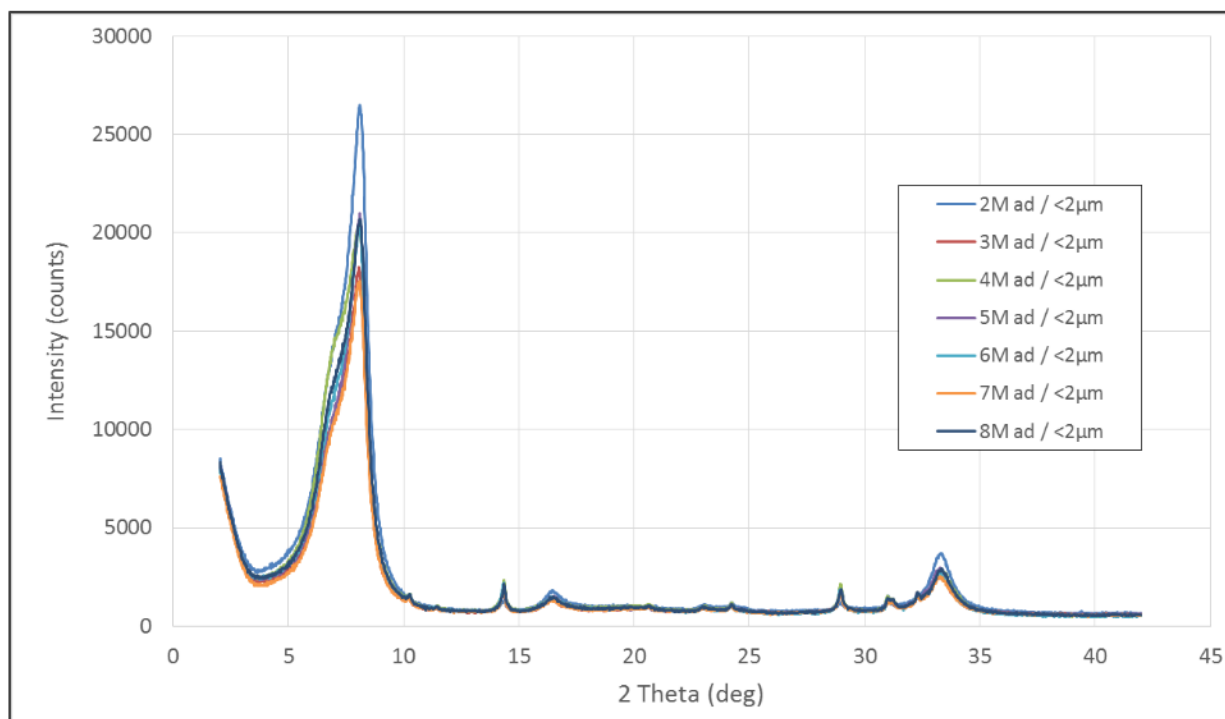


Figure 7: Comparison of clay XRD patterns of the $2\mu\text{m}$ fraction from the Queensland bentonite Mine 5 D deposit.

The $<2\mu\text{m}$ fraction of the Queensland Bentonite Mine 5D bentonite consists dominantly of Na-montmorillonite (Figure 7). The composition of the montmorillonite is remarkably consistent over the full range of tested material. Additionally a smaller amount of divalent cations (Ca^{2+} , Mg^{2+}) with two layers of water molecules are present in the interlayer positions. Carlson (2004) detected exactly this type of variations of d-values using Wyoming montmorillonite samples in a comparative study of various montmorillonites.

Formerly measured presence of a Ca-montmorillonite dominated $<5\mu\text{m}$ fraction (Holl 2016a, 2016b, Appendix 04 and 05) could not be confirmed. The earlier used raw 5D bentonite seems to be contaminated with external Ca^{2+} supply or Ca-montmorillonite either during the drying/processing of the material in the mine area (the 5A bentonite shows Ca rich montmorillonite phases in the clay fraction, see Appendix 01) or during the storage period in the laboratory of the School of Chemical Engineering, UQ.

2.2.2 Geochemistry

2.2.2.1 XRF measurements

The same nine bulk bentonite samples, which were analyzed to determine the mineralogical content (compare Section 2.2.1.1), underwent an X-ray Fluorescence (XRF) spectrometry analysis to detect major and trace element concentrations obtained from aliquots of the samples. Sample preparation, XRF measurement parameters, and the analytical results are reported in detail by Raftery (2018) (Appendix 01).

A summary of the major element geochemical analysis of the specification sheets (Appendix 06) of the two major bentonite providers in Queensland is shown in Table 5. Figure 8 shows an assessment of the MgO/CaO ratio based on data out of the specification sheets of the bentonite materials. Results of our own geochemical analysis of the three Amcol bentonites are also plotted in the graph. Variations within the MgO/CaO ratios of the company provided data and our own measurements can be

explained by slightly different mineralogical compositions within the bentonite beds depending on their position in the mine site. The different bentonite deposits are mined at various pits on the mining lease (compare Appendix 04). The scattering of the data seems to be similar to the distribution of the results published by Scogings (2014). He compared MgO/CaO ratios from up to 10 bentonite beds mined at this location and concluded that the chemistry of the bulk bentonite is variable depending on the mineral mixture within the rocks (Figure 9). High MgO/CaO whole-rock geochemical ratios are characteristic for the bentonite deposits of the Queensland Bentonite Mine and elevated CaO values are triggered by rarely occurring minor amounts of gypsum within bentonite beds (compare data of the 5B deposit in Table 2 and Figure 2).

AMCOL	5A	5B	5D	SIBELCO	Trubond	Trufeed	Trugel 100
major element chemistry (%)				major element chemistry (%)			
SiO ₂	62.8	71.4	59.6	SiO ₂	63.6	61.5	63.8
Al ₂ O ₃	17.4	14.0	18.5	Al ₂ O ₃	14.6	17.9	13.6
TiO ₂	0.7	0.3	0.7	TiO ₂	0.4	-	0.3
Fe ₂ O ₃	3.0	2.2	3.2	Fe ₂ O ₃	2.8	2.2	2.8
CaO	0.6	1.8	1.1	CaO	0.3	0.2	0.2
Na ₂ O	1.5	2.1	1.8	Na ₂ O	1.3	1.0	2.3
MgO	1.8	1.9	2.3	MgO	2.0	1.7	2.0
K ₂ O	1.2	0.7	0.7	K ₂ O	0.5	0.4	0.2
physical properties				physical properties			
bulk density (t/m ³)	0.9	0.9	0.9	bulk density (t/m ³)	1.0	1.2	1.0
CEC (meq/100ml)	80	60	80	CEC (meq/100ml)	80	70	80
moisture content (%)	13	13	14	moisture content (%)	10	13	10

Table 5: Major element chemistry, bulk density, CEC and moisture contents of the major bentonite provider technical specification sheets (Appendix 06).

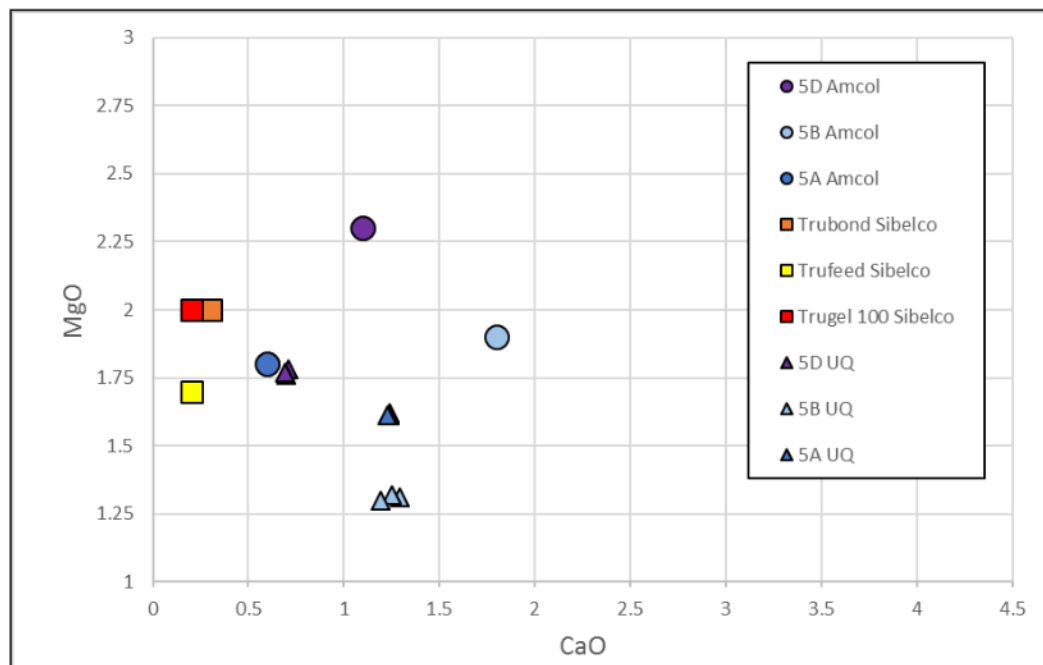


Figure 8: MgO/CaO plot of six different bentonite materials. Three samples of each of the major bentonite providers in Queensland (Amcol Australia Pty Ltd: circles; Sibelco Australia Pty Ltd: squares) based on their technical specification sheets

and nine measurements of the three bentonite materials provided by Amcol which were used in this study (triangles).

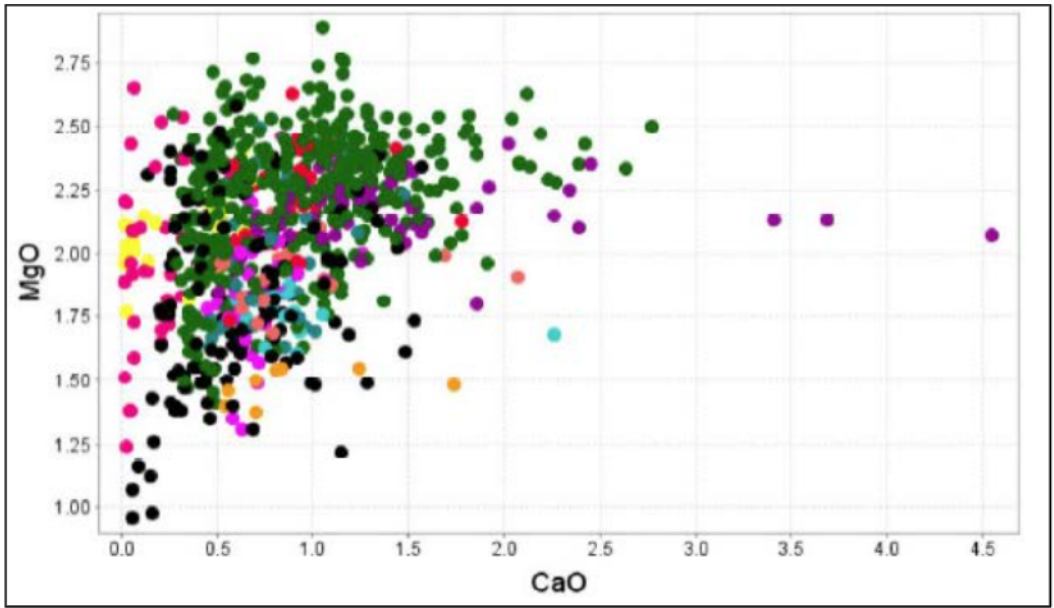


Figure 9: MgO/CaO plot of different bentonite beds (colour coded) in the Queensland Bentonite Mine (Scogings 2014). Elevated CaO values (purple dots, right hand side of the plot) are due to minor gypsum contents.

Figure 10 shows the Na₂O/CaO ratios of the six different bentonite materials, organized in the same way as in Figure 8. A similar scattering is detectable in the plot of the MgO/CaO ratios. In both plots the samples of Sibelco Australia Pty Ltd show a very constant, very low CaO concentration which is most likely caused by processing (“sodium activation”) of the bentonite material. This processing uses an ion exchange process to create a uniform distribution of sodium in order to increase its water absorption performance. Sibelco Australia Pty Ltd decided not to provide raw samples for the proposed analytical program as already mentioned in Section 2.1.

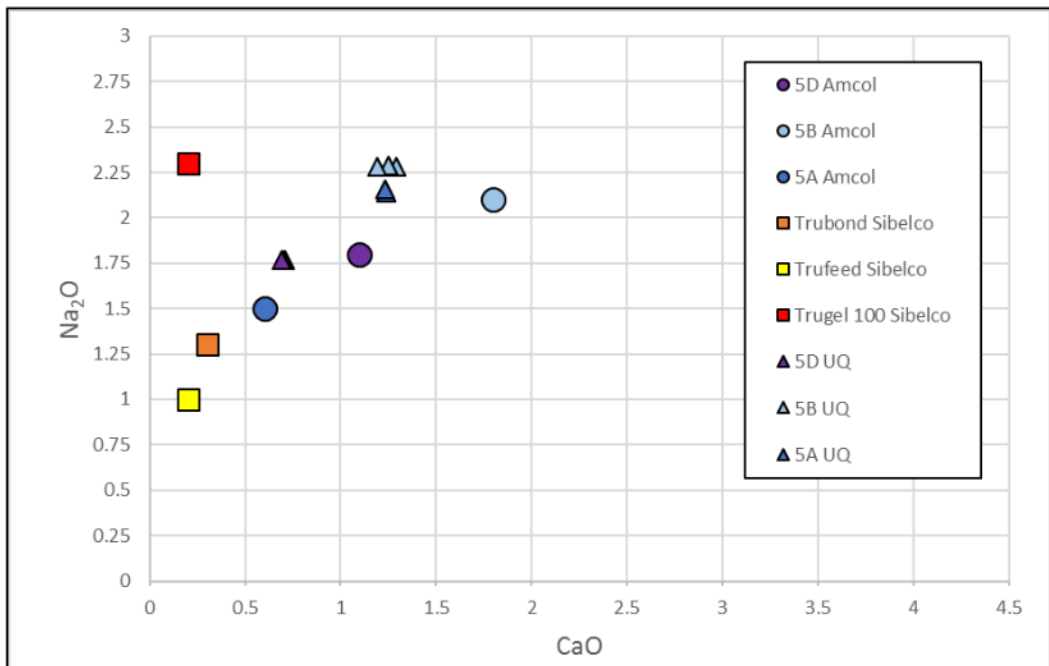


Figure 10: Na₂O/CaO plot of six different bentonite materials. Three samples of each of the major bentonite providers in Queensland (Amcol Australia Pty Ltd: circles; Sibelco Australia Pty Ltd: squares) based on their technical specification sheets and nine measurements of the three bentonite materials provided by Amcol which were used in this study (triangles).

2.2.2.2 Cation Exchange Capacity (CEC) measurements

Hydration of the exchangeable cations of the tested clay minerals is the cause of the swelling of the montmorillonite content of the bentonites (Muurinen, 2011). Measurements of the CEC values allows us to compare relative swelling properties of the analyzed materials (QA/QC).

The CEC of the bentonite materials was determined by using the silver thiourea (AgTU⁺) method as described in Rayment & Lyons (2011). Sample preparation and later measurement using an Inductively Coupled Plasma Optical Emissions Spectrometer (ICPOES) was commenced at the School of Agriculture and Food Sciences, Soil Sciences, UQ.

CEC values are greatly influenced by preparation method. Milled samples will always show higher values because of the production of higher reactive surface area due to the grinding process (Rayment & Lyons, 2011). The bentonite plug production process does not involve any grinding treatment of the raw bentonite. We have chosen to use a sieved grainsize fraction (<2mm) of the raw bentonites because dispersed clays should represent natural grain (aggregate) sizes and therefore the natural reactive surface area. Therefore the results show lower CEC values than reported in the technical specification sheets. The measured values of all analyzed samples are on average 28% lower than the CEC's provided by the bentonite producers. The analytical results of the companies are most likely based on milled samples and are not representative for the use of compacted bentonite as it is used in the plug and abandonment field trials.

Table 6 shows the results of CEC measurements of the same samples used for quality assurance of the bentonite used for plug production (Section 2.2.1.2). CEC is conventionally expressed in meq/100 g which is equal to centimoles of charge per kilogram of the exchanger: cmol(+)/kg (Rengasamy & Churchman, 1999). The average CEC in Figure 11 is 56.8 ± 1.4 cmol(+)/kg and is 29% lower than the reported value of Amcol Australia Pty Ltd.

	Ca	K	Mg	Na	CEC sum
sample	cmol(+)/kg	cmol(+)/kg	cmol(+)/kg	cmol(+)/kg	cmol(+)/kg
2M	22.2	0.6	8.5	25.7	57.0
3M	19.9	0.7	8.5	25.6	54.7
4M	22.3	0.7	8.4	25.1	56.5
5M	23.1	0.7	8.6	25.8	58.2
6M	22.7	0.7	8.5	25.6	57.5
7M	20.2	0.6	8.6	25.8	55.2
8M	23.7	0.6	8.3	25.7	58.3

Table 6: Results of the effective CEC (CEC sum) of the raw 5D bentonite bulker bags used for the plug production.

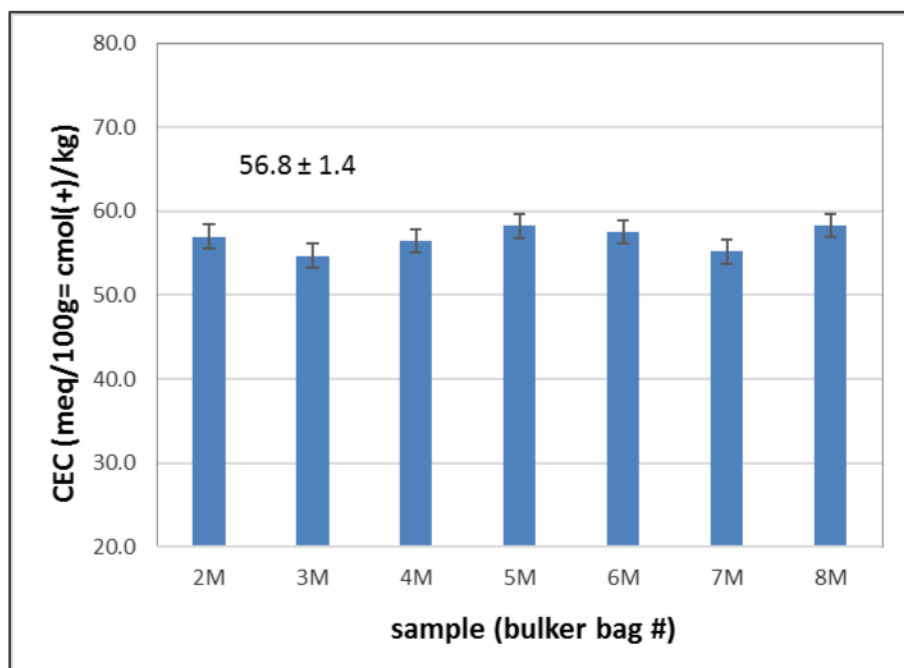


Figure 11: Effective CEC of the 5D bentonite bulker bags used for the plug production.

A second series of samples was prepared and analyzed after milling the bentonite. CEC's of all three bentonites provided by Amcol Australia Pty Ltd were measured and compared with the values out of the specification data sheets (Table 7). The CEC of the milled 5D bentonite fits with the provided CEC values. The measured values of the 5B and 5A materials are nearly 13% lower than reported.

Sample ID	Ca cmol(+)/kg	K cmol(+)/kg	Mg cmol(+)/kg	Na cmol(+)/kg	CEC (sum) cmol(+)/kg	CEC Amcol cmol(+)/kg	difference UQ to Amcol CEC (%)
5A-1	23.8	0.8	12.2	33.5	70.3	80.0	12.9
5A-2	22.6	0.7	12.4	33.3	69.0		
5B-1	5.2	0.4	6.9	40.1	52.6	60.0	12.7
5B-2	5.1	0.4	7.0	39.7	52.2		
5D-1	30.3	0.8	13.1	34.7	79.0	80.0	0.4
5D-2	31.1	0.9	13.3	35.2	80.4		

Table 7: CEC measurement results of the three analyzed bentonite materials and comparison with the CEC values of the provided specification data sheets.

The CEC measurements are confirming that the 5D bentonite deposit is the most promising candidate for delivering best swelling performance of all tested materials. The QA results delineate consistent Cation Exchange Capacity performance of the 5D bentonite used for the plug production.

2.2.3 Mechanical properties testing

The geomechanical data used in the pre-existing modelling of the hydro-mechanical behaviour is based on a literature review and includes high uncertainties. Data gathering using oedometer tests, direct shear tests (after swelling of the plug) and conventional axial loading tests (unconfined compressive strength and triaxial cell tests with compacted plugs) will increase the quality and robustness of the modelling approach. In order to gather the parameters required to simulate the hydro-mechanical behavior of bentonite plugs under the influence of water, a staged laboratory program was implemented.

Compressed bentonite samples, using two levels of compression (9.2 and 18.3t), with and without the addition of the polymer PVP (polyvinylpyrrolidone) were tested in the laboratory. The laboratory study involved two main set-ups:

- An oedometer set-up to conduct swelling tests at constant normal stress observing the residual swelling for different stress states.
- Direct shear tests to determine strength parameters at different hydration states (the results of the oedometer tests are required to define the hydration state at which the mechanical tests are conducted).

The tests were conducted in the laboratories of the Geotechnical Engineering Centre at UQ to create high quality data input for the theoretical prediction of bentonite plug reliability. Sample preparation and analytic methodology is described in detail by Scheuermann & Holl (2017, Appendix 07).

Swelling tests were conducted to characterize the swelling behavior and to quantify the swelling pressure:

- The final swelling strain was 20% larger for raw samples than for PVP treated samples.
- Samples compressed to a higher level produced 30% larger swelling strain.
- Swelling pressure varies between 1580 kPa (229 psi) and 1740 kPa (252 psi) with the higher swelling pressure for the sample with the higher compression weight of 18.3 t. The treatment of the sample seems not to influence the swelling pressure.

Shear tests were implemented to determine the shear strength of PVP treated and untreated bentonite samples. The results are shown in Figure 12.

- PVP treated samples show a much larger frictional behaviour than raw samples. The friction angle varies between 6.0° for 9.2 t compressed samples and 6.7° for 18.3 t compressed samples. The friction angles for raw samples are much smaller, with 1.4° for 9.2 t compressed samples and 1.8° for 18.3 t compressed samples.
- Samples prepared with 18.3 t weight show a much higher shear strength than samples prepared with 9.2 t weight, regardless of the material composition. For PVP treated samples, the difference in shear strength is considerably larger than for raw samples. The difference is visible in both friction angle and cohesion, though the influence on cohesion is significantly larger.

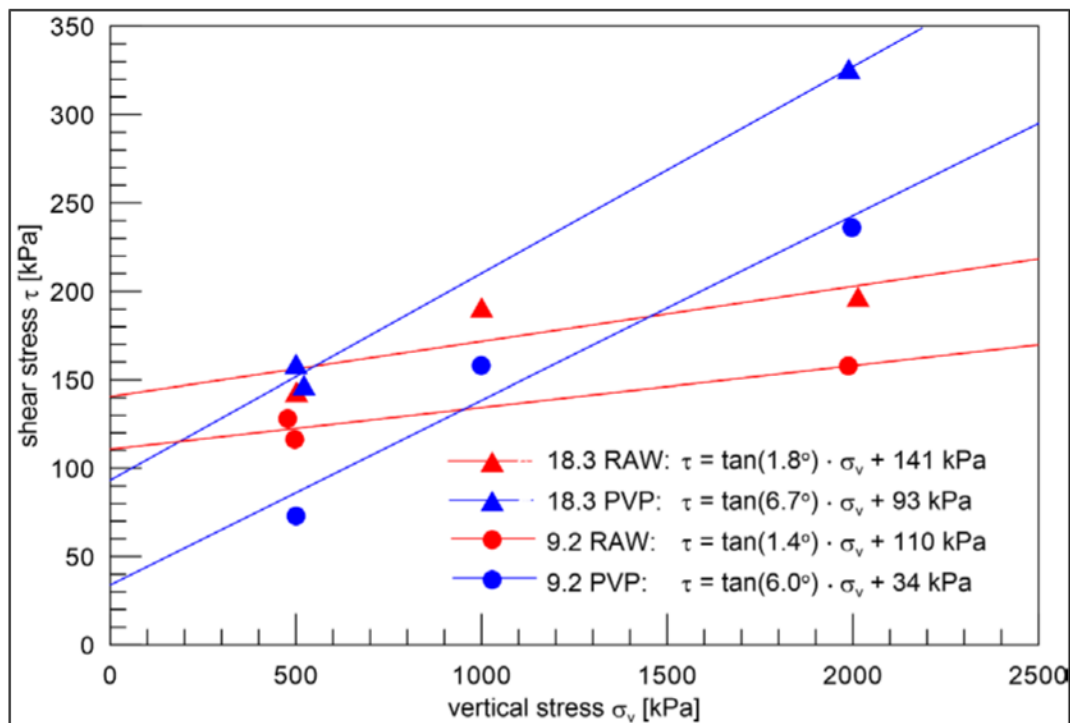


Figure 12: Comparison of the shear test results together with the Mohr-Coulomb failure criteria (Holl & Scheuermann, 2018).

The shear strength parameters determined were used as input for refining the mechanical properties in the hydration model, which was used to predict the swelling and shear strength performance of the installed plugs under well conditions (detailed in Chapter 4).

2.2.4 Small and Ultra Small Angle Neutron Scattering (SANS and USANS)

SANS and USANS techniques were used to characterize nanostructures in the bentonite materials (with and without a polymer binder, PVP) used for the plug production. These measurements give insight into changes in the microstructure as a function of moisture content, strain and other chemical and physical perturbation. Sample preparation and analytical methods are described in detail in Blach & Holl (2018, Appendix 08). The analytical approach shows:

- Evolution of structural changes in the plug material as a function of moisture and polymer content
- Evolution of porosity changes and the effect of moisture on the plug material
- Nano-structures in the plug material most affected by the moisture and polymer addition
- Mechanism of self-healing

We have exposed the samples to hydration by evaporating water and then applied CD₄ methane at a Zero Average Contrast (ZAC) pressure (about 7000psi) to measure the accessible and inaccessible pores and channels. The data shows that introduction of moisture has an immediate effect on the smallest pores in the raw bentonite plug, with swelling preventing access by the methane; however the larger network appears to be little affected by the addition of the moisture. The addition of a binder (PVP) to the plug creates a greater number of open pores in the micron and above size regime, indicating that the polymer is vital in creating larger channels, which aids the movement of moisture throughout the plug, at the expense of sealing the smallest ones. This suggests that the polymer binder helps in the hydration process in the clays and makes the confined structure more stable.

The process of plug manufacturing produces a chaotic system of aggregates in the sample, which form packed clusters 130nm in size. Addition of moisture disturbs this structure. Addition of water to the plug material showed that at 18 wt% a dual layer of water has formed in the montmorillonite interlayer space of the clay, separating the montmorillonite layers by 17 Å. Increase to 33 wt% of water has added an extra layer which creates a basal spacing of 19 Å. The clay hydration with vapour and directly deposited liquid appear to delaminate some of the clay affecting the fractal index at the micron sizes.

These results helped to refine the hydration model developed in the project and allowed better prediction of the swelling behavior of bentonite plugs under wellbore conditions.

3 Failure mode and bentonite performance modelling (by Brian Towler, CCSG)

A detailed summary of the failure mode modelling conducted is given in Towler et al. (in prep.) (see Appendix 09).

In sealing a well-bore, hydrated bentonite could fail by several means. We have examined two principal modes of failure; (a) frictional failure at the wall, where the entire plug loses its grip on the wall of the well-bore, and (b) internal shear failure where the plug fails internally because the shear strength has been breached. A third failure mode has been identified, which will not be discussed in this report, but in subsequent publications. This failure mode occurs when the applied pressure is increased slowly and the fluid begins to bleed through the plug. In this case, the failure tends to occur at or near the wall, where the bentonite plates tend to be aligned parallel to each other. This third failure mode requires some fundamental theory, which needs to be developed in some detail and examined separately. The first two failure modes have been examined in the attached paper draft, shown in Appendix 9. These results are summarized here.

Frictional Failure

Towler and Ehlers (1997) have derived the equation for frictional failure. They have shown that if there is a column of water and a column of gravel on top of a hydrated bentonite plug then the pressure in the formation, required to overcome the frictional force at the wall will be given by:

$$P = \frac{2K_b \rho_b g H^2}{D} + \frac{4K_b \rho_w g L_w H}{D} + \frac{4K_b \rho_g g L_g H}{D} + \rho_w g L_w + \rho_g g L_g + \rho_b g H$$

Equation 1

Equation 1 does not take into account internal swelling pressure created by either osmotic pressure of the hydrating clay or the inter-crystalline forces created by water molecules forming around the sodium ions between the crystalline platelets. The internal swelling pressure acts perpendicularly to the walls causing an outward pressure on the pipe walls. When this pressure is multiplied by the coefficient of friction, K_b , it gives rise to an additional frictional force that must be overcome. But the outward swelling pressure acts over an area of πDH , whilst the dislodgement pressure acts over $\pi D^2/4$. Consequently, equation 1 becomes:

$$\Delta P = \frac{2K_b \rho_b g H^2}{D} + \frac{4K_b \rho_w g L_w H}{D} + \frac{4K_b \rho_g g L_g H}{D} + \frac{4K_b H P_{swell}}{D} + \rho_w g L_w + \rho_g g L_g + \rho_b g H$$

Equation 2

There is very little published data for internal swelling pressure, but Bucher and Müller-VonMoos (1989) have made some measurements and postulated that the swelling pressure is an exponential function of the hydrated density, which in turn has been shown to be a function of the moisture content. Thus the internal swelling pressure will be given by the general equation:

$$P_{swell} = \epsilon e^{k\rho_b}$$

Equation 3

Because the clay platelets reorient themselves in the direction parallel to the pipe walls, which for this case the vertical direction is assumed. In this case, the internal swelling pressure pushes out in the horizontal direction and increases the frictional force against the vertical walls. If we include that term in equation (4) it becomes:

$$P = \frac{2K_b \rho_b g H^2}{D} + \frac{4K_b \rho_w g L_w H}{D} + \frac{4K_b \rho_g g L_g H}{D} + \frac{4K_b H \epsilon e^{k\rho_b}}{D} + \rho_w g L_w + \rho_g g L_g + \rho_b g H$$

Equation 4

Thus the pressure required to overcome the frictional forces may have a parabolic relationship with the height of the plug. This means that if we measure the pressures that cause plugs of different heights and diameters to fail due to the failure of the frictional forces and we plot the data as:

$$\Delta P \pm \rho_w g L_w \pm \rho_g g L_g \pm \rho_b g H \text{ versus } \frac{2 \rho_b g H^2}{D} + \frac{4 \rho_w g L_w H}{D} + \frac{4 \rho_g g L_g H}{D} + \frac{4 H \epsilon e^{k\rho_b}}{D}$$

Then the slope of this plot will be the coefficient of friction, K_b .

Shear Failure

The plug can also fail in shear; and if the shear strength is less than the frictional strength, this failure mechanism will dominate. The shear failure is postulated to occur around an internal cylinder.

In our paper, as shown in Appendix 9, the plug will fail by shear when:

$$P = \frac{4\tau_s H}{D} + \rho_b g H + \rho_w g L_w + \rho_g g L_g$$

Equation 5

So the pressure to overcome the internal shear forces is directly proportional to the height of the plug, H , and the internal shear strength, τ_s , and, as with the frictional strength, is inversely proportional to the diameter of the plug, D .

Applying these two mechanisms together, for short plugs the frictional forces dominate; and the plug strength increases parabolically with the height of the plug. But eventually the internal shear strength becomes less than the frictional strength. So for long plugs the plug strength becomes linear with the plug height.

Analysing Laboratory Failure Data

The equations derived above suggest that the failure pressure will be inversely proportional to plug diameter and, depending on the failure mode, can be proportional to the plug height or square of the height. However, for long plugs, it is postulated that the failure pressure will be proportional to the plug height. Towler and Ehlers (1997) only considered the case where it was proportional to the height squared but others (Englehardt et al 2001, Clark and Salsbury 2003) assumed the failure pressure was more likely to be linear with height. Towler and Ehlers (1997) neglected consideration of swelling pressure, which can be more important than plug weight in the frictional term. They also neglected the fact that shear strength can be less than frictional strength for long plugs. All these factors suggest that plug strength is likely to be proportional to plug height and inversely proportional to plug diameter. So the linear equations above can be summarized as:

$$\frac{(\Delta p \pm \rho_b g H) D}{H} = C(\tau_s, K_b, \rho_b)$$

Equation 6

If the plug fails due to friction created by the swelling pressure, then $C = 4K_b.P_{swell}$. On the other hand, if the plug fails due to internal shear strength the value of C depends on the geometry of the shear failure. For cylindrical shear failure around the perimeter the value is $C = 4\tau_s/\pi$. Note that the linear frictional parameter, $K_b.P_{swell}$, is equal to $C/4$, while the cylindrical shear strength, τ_s , is equal to $C\pi/4$. But τ_s and K_b are functions of moisture content (M%) salinity (S%), absolute pressure (p) temperature (T) and hydration time (t_h). So Equation 6 can be written:

$$\frac{(\Delta p \pm \rho_b g H) D}{H} = C(M\%, S\%, p, T, t_h)$$

Equation 7

These relationships were investigated with available laboratory data. The first three data sets from Bell et al. (2009), Koelling et al. (2011) and Anderson et al. (2013) were measured on J55 steel casing with outside diameter (OD) of 4.5-inches and interior diameter (ID) of 4-inches. The final data set of Morteza pour (2016) was measured on steel casing of two different sizes, the first being 7-inch OD and ID of 6.366 inches, and the second having an OD of 5.5-inches and ID of 4.778-inches. The density of the hydrated plugs depends on the final moisture content and neither density nor moisture content were measured for the first three data sets. However, using some assumptions based on the plug and casing geometry, a moisture content of 35% and a density of 1.65 g/cc were assumed.

The first item to note is that, in laboratory trials at the University of Wyoming, whenever a bentonite plug was breached through excessive pressure drop the plug was shown to be healed again when tested even two days later. This healing ability was demonstrated over many years of laboratory tests. In fact, when each plug was allowed to heal for as little as two days, the plug not only healed the

breach, it was stronger next time. Thereafter, the continually re-healed plugs gained in strength as the total hydration time increased. Bell et al (2009) measured an average pressure containment of 20 psi/ft with a range of 10-38 psi/ft. However, the failure gradient increased with time at a rate of 0.47 psi/ft/day. It was still increasing when they ceased testing after 71 days for plugs 1 and 2 and after 44 days for plugs 3 and 4. The data of Bell et al (2009) is shown plotted in Figure 13 as the failure gradient in psi/ft versus hydration time.

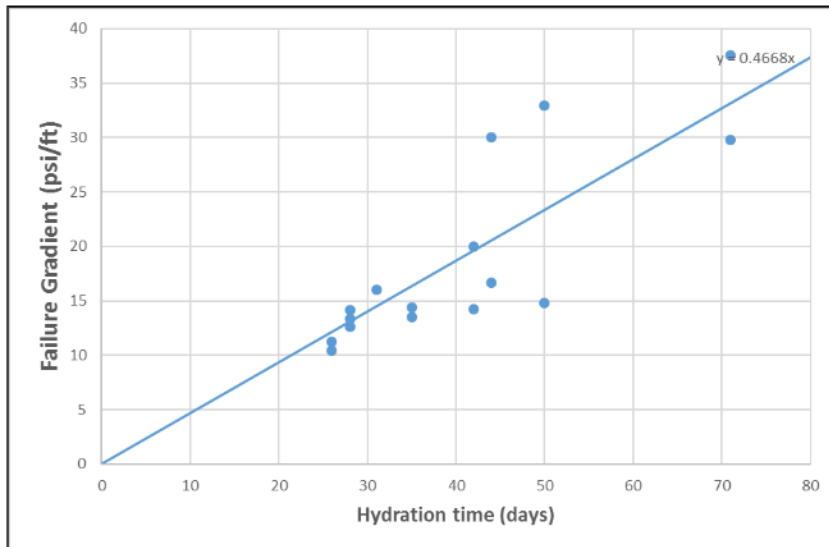


Figure 13: Failure gradient as a function of hydration time. Data of Bell et al. (2009).

In another set of experiments from Anderson et al. (2013), the effects of salinity and temperature were measured. The room temperature (68°F) data is shown plotted in Figure 14 below. In general, as salinity and temperature increase the strength of bentonite plugs decreases. However, all of these data were gathered at atmospheric pressure, and it is expected that the strength of the plug will increase as the containment pressure increases. So as the depth of the well gets very deep, the temperature of the plug will increase but so too will the pressure due to the column of fluid above the plug. These two effects will partially off-set, but currently it is not known to what extent this will happen. This needs further investigation. In Figure 14 it can be seen that, while the plugs were weaker in saline water of salinities of 10,000 ppm to 20,000 ppm, they still reached failure gradients of 23 psi/ft after 120 days of hydration, after which they tended to increase further. Plug 3 was hydrated in fresh water directly from the University of Wyoming faucet (which is connected to the Laramie city water supply) and can be compared directly to the experiments of Bell et al (2009), shown in Figure 13. For those experiments plugs 1 and 2 were still increasing in strength after 71 days of hydration. The Anderson et al. (2013) data for plug 3 plateaus in strength after 71 days, but later increases again, plateauing at a strength of 180 psi/ft after about 175 days. It is possible that the first plateau after 71 days happened because the plugs were not kept properly moist during a period of inactivity. But once testing resumed they were re-hydrated and the plug strength began increasing again. The plugs hydrated in saline water were weaker than the fresh-water plugs, but increased in strength to about 37 psi/ft after 175 days. This means that a hundred-foot plug that is 4-inches in diameter could contain at least 3700 psi.

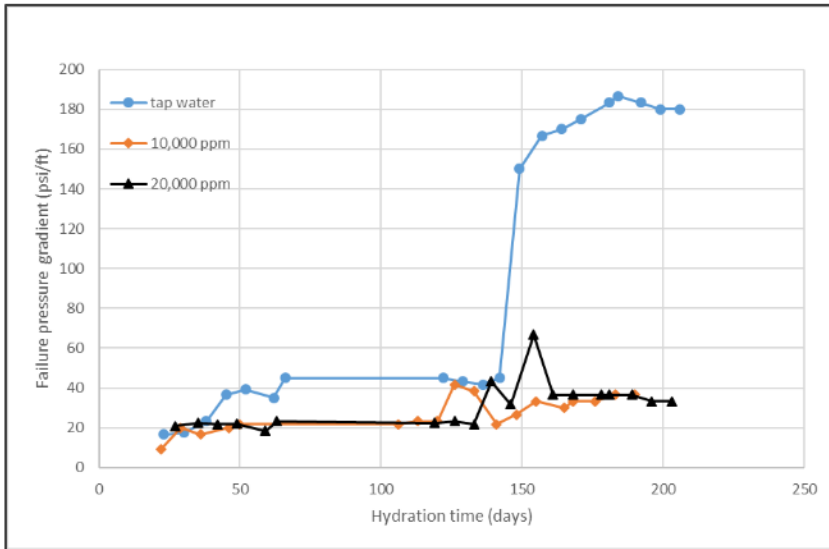


Figure 14: Effect of salinity on failure pressure gradients as a function of hydration time, data of Anderson et al. (2013).

Koelling et al. (2011) also tested the effect of salinity at room temperature. This data is shown in Figure 15. Their data clearly showed that the bentonite plug that was hydrated in fresh water was stronger. Moreover, the plugs hydrated in fresh water were stronger after the plugs had failed and continued to increase in strength as time increased. At higher salinities there were some inconsistencies, making the results not easy to interpret; but this is a subject for further investigation.

Towler et al (2008) reported failure data for a series of short plugs, which means that the plugs likely failed due to frictional failure. Consequently, K_b was calculated using equation (1). The hydration time was relatively short and the plugs were unlikely to be fully hydrated and so not at full strength. They found that the friction factor was a strong function of moisture content as shown in Figure 15. As the moisture content increases the notional friction factor decreases. These calculations made an assumption about the failure mechanism (frictional failure), but, even though the data does not indicate what is the actual failure mechanism, frictional failure is a reasonable assumption given that the plugs were very short.

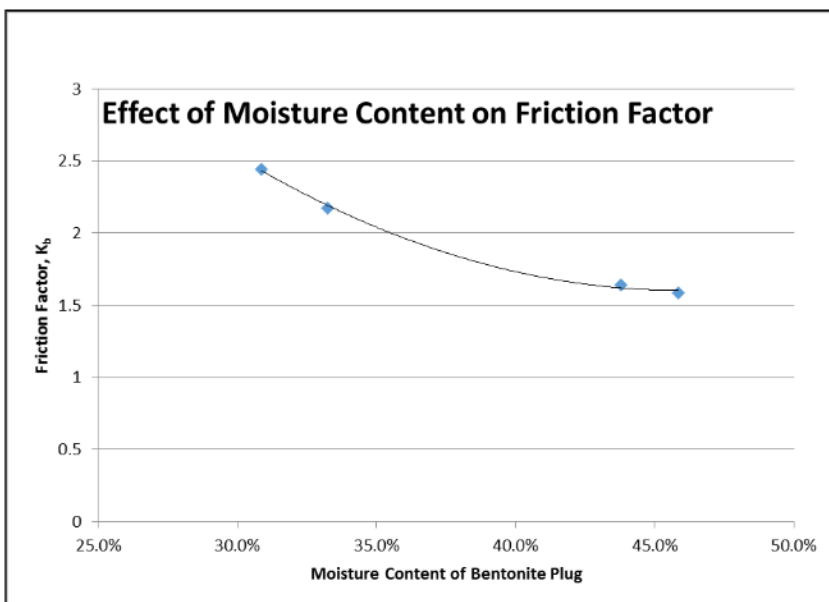


Figure 15: Effect of Moisture Content on Friction Factor, data of Towler et al. (2008).

Lab Tests with Queensland Bentonite

Laboratory tests have also been conducted with bentonite from the 5D layer in Amcol's Gurulmundi mine near Miles in Queensland, Australia. This bentonite is similar to Wyoming bentonite in that it primarily consists of sodium montmorillonite. Detailed technical information on the composition of the Queensland bentonite from the Gurulmundi mine has been given in Chapter 2 of this report. The swell tests and pressure containment from preliminary results suggest that this bentonite has similar strength to the MX-80 bentonite from Wyoming. The initial tests were conducted at two different plug diameters of 0.416 ft and 0.573 ft, and plug heights that range from 0.67 ft to 2.21 ft. Failure is being generated using a circular plate force which forces the plugs to fail either due to friction at the wall (either due to plug weight or swelling pressure) or shear failure at the wall. The equipment used is more fully documented in Towler et al. (2015). The measured pressure containment is in the range of 12-22 psi/ft, which is similar to the range measured for the Wyoming bentonite.

Further Analysis

At this stage it has been established that bentonite plugs can fail due to shear or frictional failure and each of these gives rise to two types of failure. Frictional failure can be linear or parabolic depending whether the friction arises out of internal swelling (which is linear with plug height) or bentonite plug weight (parabolic behaviour). The shear strength will be linear with plug height. It has also been demonstrated that plug strength is a function of hydration time, final moisture content and water salinity. The tests used so far have not identified the mode of failure but we can use the equations developed and the data presented to calculate the key parameters for the case of each mode of failure. For the data of Bell et al. (2009) the key parameters have been calculated for each test. The maximum values were obtained after 71 days but the data of Anderson et al. (2013) suggests that these plugs have not achieved full strength even after 71 days of hydration. But at that time the parabolic K_b was 1.04, the linear frictional strength $K_b.P_{swell}$ was 3.07 psi, the cylindrical shear strength was 9.65 psi, and the planar shear strength was 3.07 psi. Using the maximum values of Anderson et al. (2013), the plugs hydrated in tap water reached maximum strength after 184 days. At that time the parabolic K_b was 7.25 the linear frictional strength, $K_b.P_{swell}$ was 15.6 psi, and the cylindrical shear strength was 48.9 psi.

The tap water data of Bell et al. (2009), Anderson et al. (2013), Koelling et al. (2011), and Morteza pour (2016) can be combined into one plot to compare different researchers' results. This is shown in Figure 16. In this plot the linear strength parameter, C , is plotted versus hydration time. Even though none of the bentonite in these tests has reached full strength and there is significant scatter in this data, the results show a remarkable consistency. Note that the data of Bell et al. (2009), Koelling et al. (2011) and Anderson et al. (2013), was measured on Wyoming bentonite obtained from the northern Wyoming mines of Black Hills Bentonite. However, the data of Morteza pour (2016) was measured on Queensland bentonite obtained from Amcol's Gurulmundi mine north of Miles, using different techniques. However, the results are remarkably similar to the results for the Wyoming bentonite. The composition of Queensland bentonite shows that the 5D zone from the Amcol mine is primarily sodium montmorillonite, which is postulated to give the best expansive behaviour needed for sealing operations.

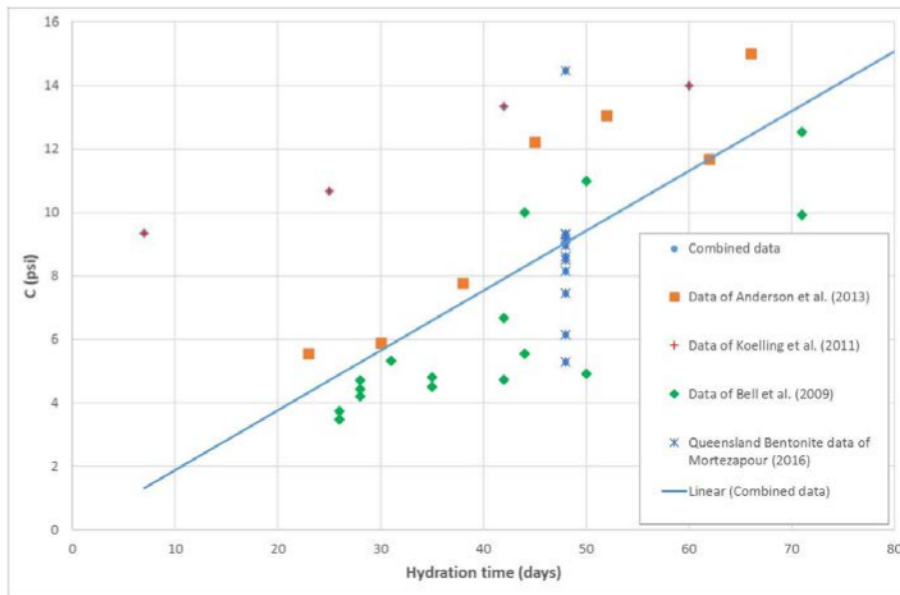


Figure 16: Linear Bentonite Strength Data as a Function of Hydration Time.

Conclusions of the modelling analysis

The equations used here and derived in the appendix have determined that when hydrated bentonite plugs fail due to friction at the walls created by internal swelling pressure or through internal shear failure, the resulting failure pressure is linear with height, coefficient of friction or internal shear strength, and inversely proportional to plug diameter. On the other hand, if the friction at the walls is created by plug weight then the failure pressure is a function of H^2/D . However, in this case, the frictional strength is increasing parabolically with height, and, at reasonable plug heights, the frictional strength becomes greater than shear strength, and failure will occur due to internal shear failure, which will also make the failure pressure a function of H/D . This suggests that plug strength is usually a linear function of H/D . Moreover, the coefficient of friction and internal shear strength are dependent on final moisture content of the hydrated plug, the salinity of the hydration water, pressure, temperature and hydration time. Hydrated bentonite plugs appear to reach maximum strength after at least 184 days of hydration. However, this will depend on the plug's geometry. The plug strength decreases in saline waters, but, at up to 30,000 ppm, the plugs still appear to have adequate strength to properly seal formations. From very limited data, shown here, Queensland bentonite, from the 5D zone of the Amcol mine, appears to have similar plugging strength to Wyoming bentonite.

4 Ranking of the bentonite material based on mechanical dislodgment pressures

The three different bentonite materials tested within this program were ranked by a comparison of mineralogical (Section 2.2.1), geochemical (Section 2.2.2), geomechanical (Section 2.2.3) properties and finally their mechanical dislodgment performance (Section 4.1).

Bentonite plugs with a diameter of 3.5" (19cm high) and 5.5" (21.5cm high) are produced in the laboratory of the School of Chemical Engineering, UQ using a custom built hydraulic vertical bentonite plug press (Figure 17). A hydraulic pressure of 2400psi is applied during the production process, which is equal to a 14.2 tons compression weight for the 5.5" plugs.



Figure 17: Hydraulic vertical bentonite plug press

The mechanical dislodgment performance was tested in two different experimental setups:

- Dislodgment of hydrated bentonite plugs using an industrial hydraulic press, and
- Dislodgment using an Instron 250 kN loading frame

4.1 Hydraulic press tests

We tested the three available bentonite materials using 5.5" PVP blended bentonites plugs. Three 7" 80cm long steel casings were loaded with one, two and three plugs of the same material each. We dislodged all nine samples at the same day after being hydrated for 42 days. A digital pressure gauge was used to detect the maximum pressure applied, which caused final movement of the hydrated plugs within the casing. A steel plate with a diameter of 161mm was installed at the hydraulic ram (Figure 18) to cover nearly the whole area of the hydrated plugs within the steel casing (161.7mm ID).



Figure 18: Industrial hydraulic Press used for primary mechanical dislodgment tests.

The results of these dislodgment tests are shown in Figure 19. The 5D bentonite samples (one, two and three plugs in 7" casings) show clearly the best dislodgment performance.

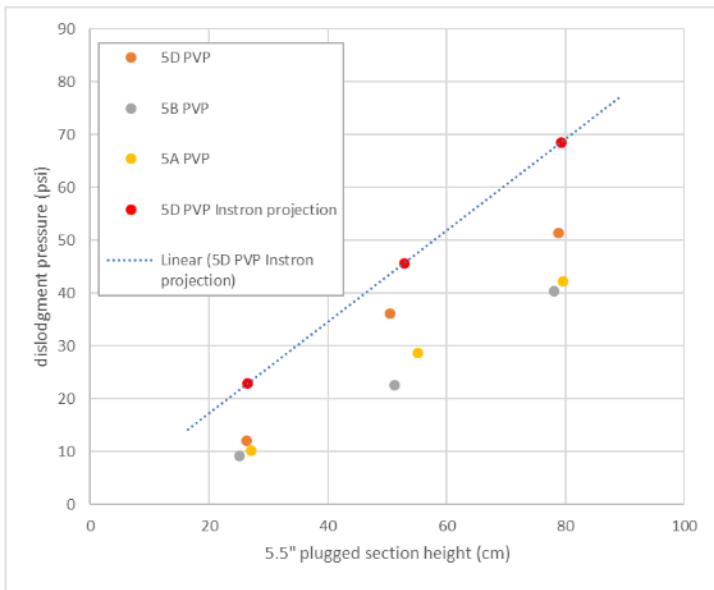


Figure 19: Dislodgment data of the three tested bentonite materials with PVP. The plugged section height was measured after 42 days of hydration.

The 5B and 5A bentonite plugs showed similar dislodgment pressures. The 5A bentonite was eventually assessed better than the 5B material because of its higher montmorillonite content and its higher cation exchange capacity (CEC) which is supposed to trigger higher swelling pressures in the long-term (see Sections 2.2.1 and 2.2.2).

Figure 19 also shows a projection of the 5D PVP blend from the load frame test which will be reported in the next chapter.

4.2 Load frame tests

The mechanical dislodgement tests were conducted using an Instron 250 kN Electro-Mechanical self-reacting loading frame (Figure 20). The 80cm long 7" steel casings with three hydrated bentonite plugs were installed in the frame using a steel clamp to centre the pipe and to allow some 20mm extra space below the sample to accommodate the dislodged bentonite.

Six samples of the 5D raw and 5D PVP treated bentonite each were hydrated for 42 days. Detailed experiment setup and measurement details are reported in Appendix 10 and Holl & Scheuermann (2018).



Figure 20: Instron 250 kN loading frame with steel clamp for central installation of the 80cm high 7" steel pipes.

The experiments using the loading frame provided much more detailed results than the trials using a hydraulic press (see Section 4.1). Gradual shear failure of the stacked plugs within the tested pipe section could be observed for the first time. A summary of all Load/Displacement data is shown in Figure 21 and Figure 22. The gradual failure is clearly to be seen in the raw bentonite samples (Figure 21 & Figure 23). The stepwise geometry is not that pronounced in the PVP blended samples (Figure 22). Final failure of PVP blended bentonite happened on average later and at higher forces than the raw samples (Figures 11 & 12 in Holl & Scheuermann, 2018).

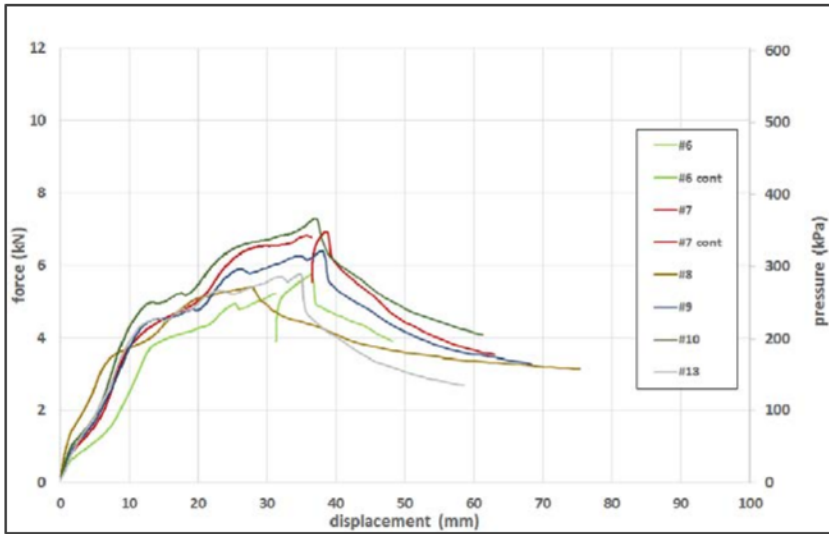


Figure 21: Comparison of Load/Displacement curves of six raw bentonite samples (5D). Continuation measurements were necessary for sample #6 and #7 after failure of the rig (Holl & Scheuermann, 2018). Sample numbers are color-coded.

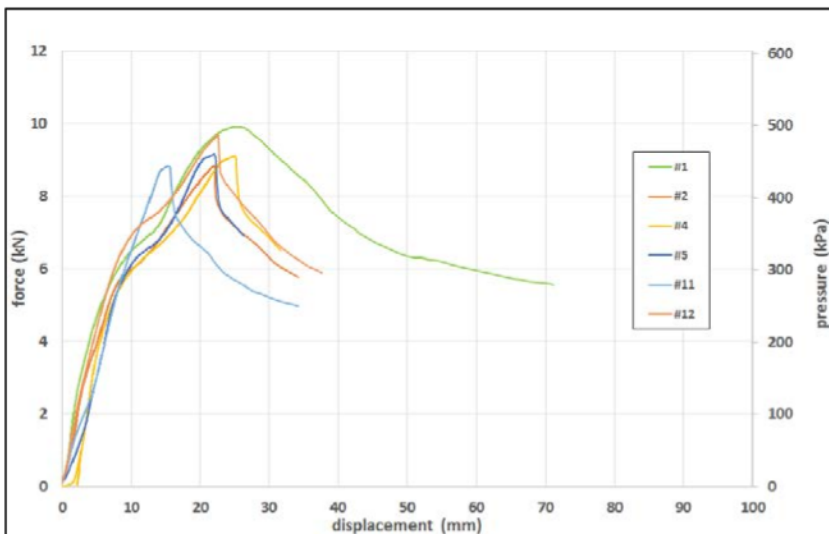


Figure 22: Comparison of Load/Displacement curves of 6 PVP blended bentonite samples (5D).

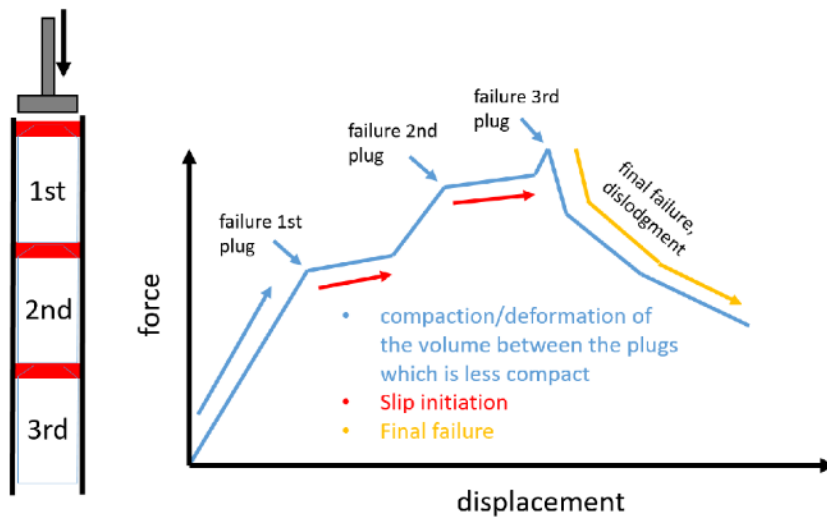


Figure 23: Schematic Load/Displacement curve showing stepwise geometry due to gradual shear failure of the three single bullet shaped plug segments (Holl & Scheuermann, 2018).

Figure 23 shows a schematic Load/Displacement curve explaining the failure process based on the curve geometry. The red areas in the sketch on the left hand side of the figure undergo compaction during the loading process of the sample. The curve geometry flattens after the first slip/failure, with continuous movement at an interval, which does show a lower increase of force during compaction of the second red area (red arrow in Figure 23). The curve is getting steeper until the next plug is shearing off. Final failure happened after dislodgment of the third plug and the complete section of plugs was pushed out of the casing (yellow arrow Figure 23). The dislodgment forces between the failure of single plugs decreases during the process, which can be explained by an overall friction reduction once single plugs have failed.

The loads were recorded in kN, but converted to units of Pound Force per Square Inches (psi). A major outcome of the experiment is the proof of different pressure regimes for raw and PVP blended bentonite plugs.

The PVP treated plugs showed dislodgement pressure gradients of $599.5 \text{ kPa/m} \pm 29.5$ ($26.5 \text{ psi/ft} \pm 1.4$), whereas the raw bentonite only went up to a gradient of $400.4 \text{ kPa/m} \pm 43$ ($17.7 \text{ psi/ft} \pm 1.9$). This is equal to 6 MPa (870 psi) for the bentonite/PVP mix or 4 MPa (580 psi) for the raw bentonite assuming a 10 m plugged section. 33% higher pressures are needed to dislodge the bentonite/PVP blended plugs compared to the raw bentonite material. PVP treated plugs show a more pronounced frictional behavior than raw bentonite samples (see detailed discussion in Holl & Scheuermann, 2018).

5 First hydraulic tests using the Well Simulator Facility

The Well Simulator Facility was commissioned in July 2017 (Figure 24). First trials were commenced after calibrating the digital pressure transducers, using the pre-set proportional pressure relief valve (nominal set pressure: 1000psi/6.9Mpa).



Figure 24: The Well Simulator Facility at the University of Queensland. 4, 6 and 8" pipes (red, blue and green) can be installed and tested up to a maximum pressure of 1000psi. Each pipe is 1m long. Sections of up to 5m height can be installed. Pressure transducers are installed at the flanges and allow pressure monitoring while pumping.

Spacers were plunged into the pipe sections to ensure that the pressure transducers in the lowermost flanges are still operational, even after filling the pipes up to 20cm below the top flanges with hydrating bentonite plugs. The pipe section were loaded with bentonite plugs by dropping them from the top into a casing partly filled with water. The first trials were commenced without installing blind flanges on the top to allow visual inspection of the failure that occurred during pressuring the plugged pipes up while pumping water into the bottom flange.

The first hydraulic test delivered very promising results. Figure 25 shows the pressure progression over time while testing ten 3.5" 5D PVP plugs (each 7.5"/19cm long) installed in a 2m long pipe section (2 joints) after 78 days of hydration. The constant pump rate during the test was 4.8l/h (1.3ml/s). We expected to see a very similar result to those provided by the mechanical dislodgement tests using a loading frame (Figure 21 - Figure 23). We could not identify exactly the same stepwise geometry due to gradual shear failure of each single plug. We registered a first distinct signal caused by slip related pressure loss after 150 seconds (158psi). There was no water production visible on top of the plugged section. Pressure was building again slowly and a couple of smaller peaks could be recorded. After 810 seconds final failure occurred at a maximum pressure of 275psi and water production was detected at the top of the plugged section.

The smaller peaks between 150 and 800 seconds are believed to be triggered by stick-slip phenomena of multiple or single bentonite plugs at different times within the plugged section. Material heterogeneities within the compacted bentonite plugs might be responsible for the "masked" dislodgment patterns compared to the patterns detected in the mechanical loading frame tests.

The pump was running a further 460 seconds after failure of the plugged section before being shut down. The shut-in pressure readings stabilized finally at 161psi, which are close to the pressure peak, which was detected at the beginning of the test.

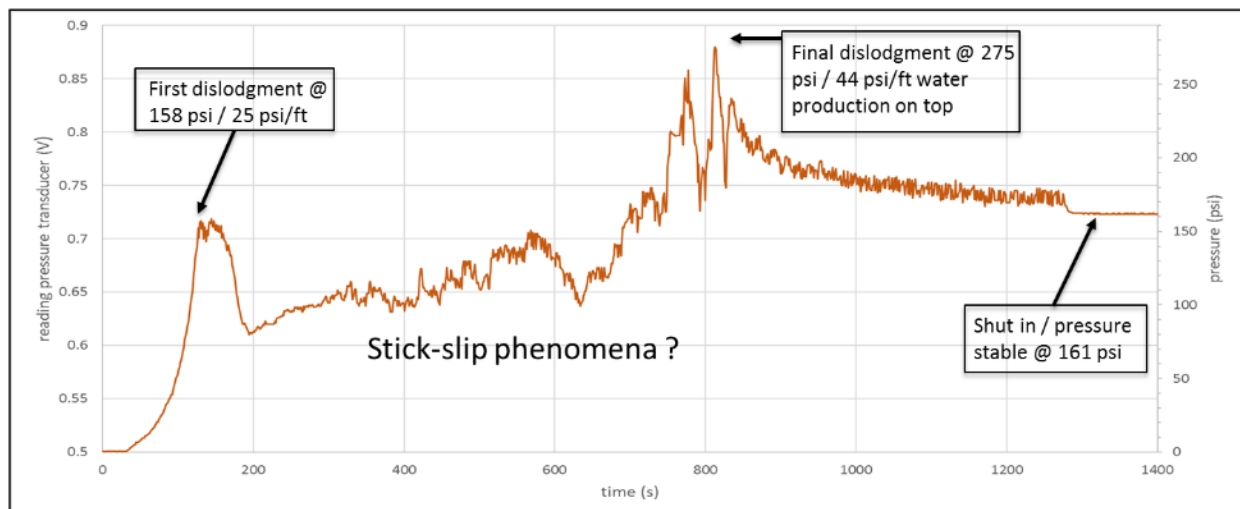


Figure 25: First hydraulic test using the Well Simulator Facility at the University of Queensland. Ten 3.5" plugs (5D PVP) installed in 2m of 4" pipe are tested after 78 days of hydration using a constant pump rate of 4.8l/h (1.3ml/s).

The second hydraulic test in the Well Simulator was conducted using the same Material (5D PVP) and the same test geometry/height as used in the first trial, but with a lower constant pump rate of 2.4l/h (0.7ml/s). The results are presented in Figure 26 and show a lot more similarity to the data derived from the mechanical dislodgement tests using a loading frame. Again, we can't assign single pressure peaks to single plugs. Failure of the plugged section caused a water leakage at 72 psi after pumping

1920 seconds. The water flow was detectable at the interface plug/steel pipe. The central hole within the plug was filled/cured with fully hydrated bentonite at this stage. Water flow through the centre of the plugged section of this sample occurred after 25 days of hydration time and failure happened at a substantially lower pressure of 32psi.

We decided to keep the tested plug interval in the simulator and tested it again a week later, but this time with a much higher constant pump rate of 36l/h (10ml/s). The results are shown in Figure 27. The rig pump was operated at 80 percent of its pumping capacity and the pressure data readings are quite noisy because of vibrations of the pump, which is directly installed beneath the rig table in contact with the metal structure. Final failure happened after a pumping period of 125 seconds at a pressure of 577psi. There was no visible water production at the top of the plugged section, instead the hydrated bentonite failed in shear mode (frictional failure) and was pushed out of the casing. The pump was shut down after 225 seconds. At this stage, 40cm of hydrated bentonite plug material (two of the ten loaded plugs) was already pushed out of the pipe and was still moving until we depressurized the system using a manual pressure relief valve and the plug movement stopped.

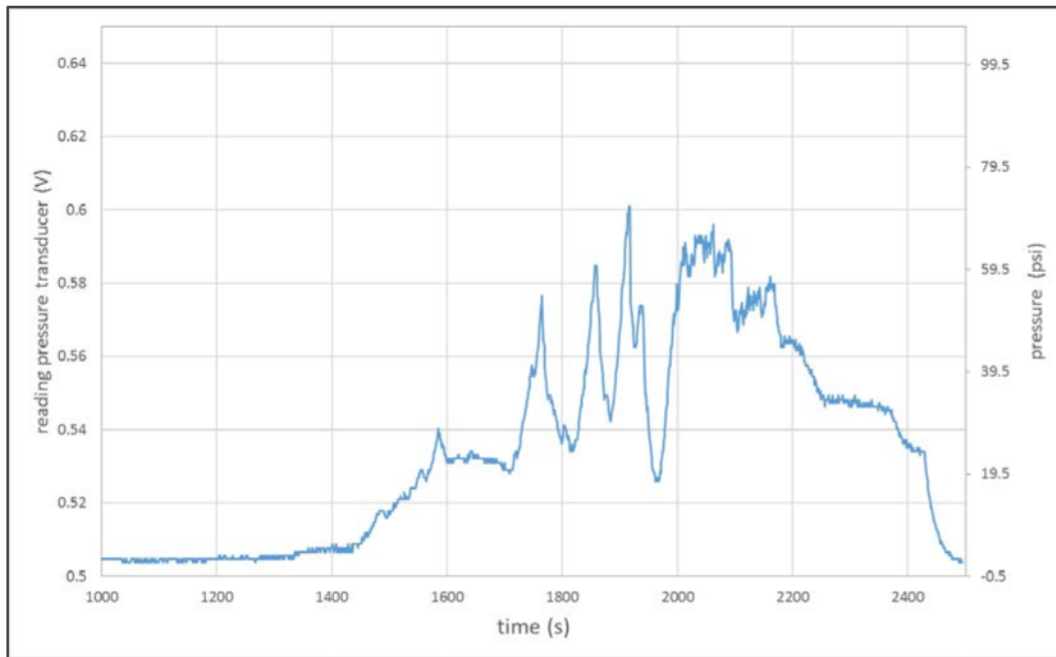


Figure 26: Second hydraulic test. Ten 3.5" plugs (5D PVP) installed in 2m of 4" pipe are tested after 51 days of hydration using a constant pump rate of 2.4l/h (0.7ml/s).

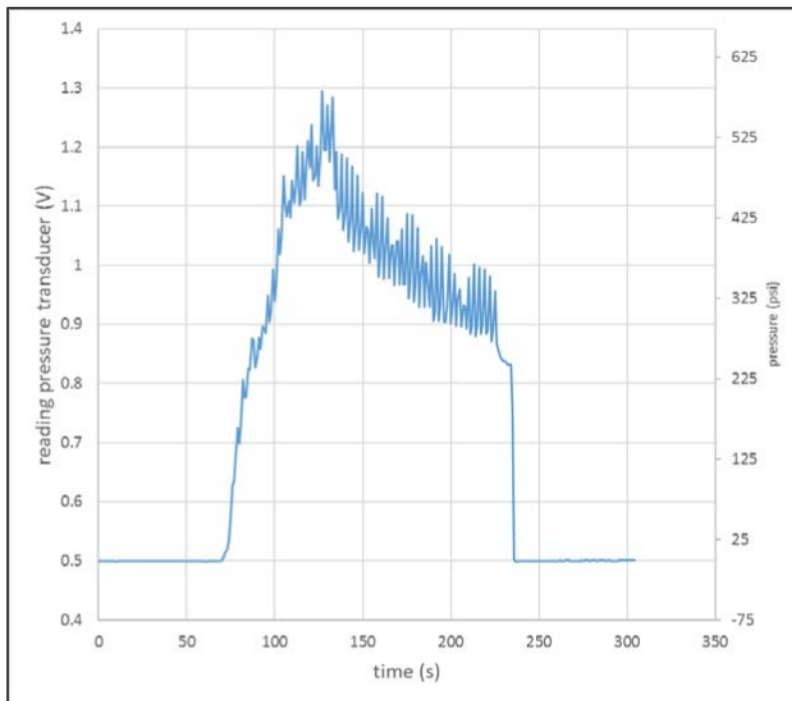


Figure 27: Second hydraulic test continued. Ten 3.5" plugs (5D PVP) installed in 2m of 4" pipe are tested after 58 days of hydration using a constant pump rate of 36l/h (10ml/s).

The high failure pressure was not triggered by the extended hydration time of 1 week. Towler et al. (in prep. / Chapter 3 and Appendix 09) have shown that maximum strength of the plugs was reached after 175 days of hydration during their experiments. The fact that the bentonite plug was pushed out of the casing shows that we are dealing with a different failure mode than observed in the two tests mentioned before. Hydrated bentonite behaves like a non-Newtonian Fluid while failing (shear-thickening). A quick pressure increase will trigger shear failure at the complete circumference of the plug at a high failure pressure, whereas slow pumping creates single micro channels at the interface plug/steel pipe at much lower applied pressures (compare also Figure 29).

The third and fourth hydraulic test have been done using single 1m pipe sections with pre-hydrated bentonite. Figure 28 shows a comparison of the 5A bentonite as PVP blend and in its raw form. They were tested after 48 days of hydration using a constant pump rate of 2.4l/h (0.7ml/s). The recorded curve geometries are quite different compared to the test results using water (blue curve in the background of Figure 28). There was a small volume of air (0.5l) at the bottom of the plugged section above the water level within the installed pipe, because of the pre-hydration procedure. This air was used to test failure in presence of gas flow. The gas volume was compressed while pumping water and the plugged section finally failed exactly as in the second test with water.

Both materials were tested after 48 days of hydration. Air bubbles were detectable at the interface plug/steel pipe (Figure 29) in the 5A PVP sample after 2300 seconds at a failure pressure of 14.5psi. The 5A raw bentonite failed in the centre and at the plug/steel pipe interface (Figure 30, after 1265 seconds and 5.8psi failure pressure). The centre of the 5A raw plug was not cured within 48 days. Direct comparison of the PVP blended bentonite with the raw material confirms that the polymer blend is 60% stronger than the raw material and the failure pressures are roughly 50% higher using water than failure pressures using air.

The decision was made to pre-hydrate plugs in single pipe sections for the long-term testing to

complete the planned experimental program in the two year project time frame. The 4" pipe sections were loaded with 5A PVP and 5D PVP bentonite plugs and stored in the laboratory with a PVC pipe extension on top of the pipe to guarantee a continuous hydraulic head on top of the plugged section. The pipes were installed on the rig after 3, 6 and 9 months hydration time and tested.

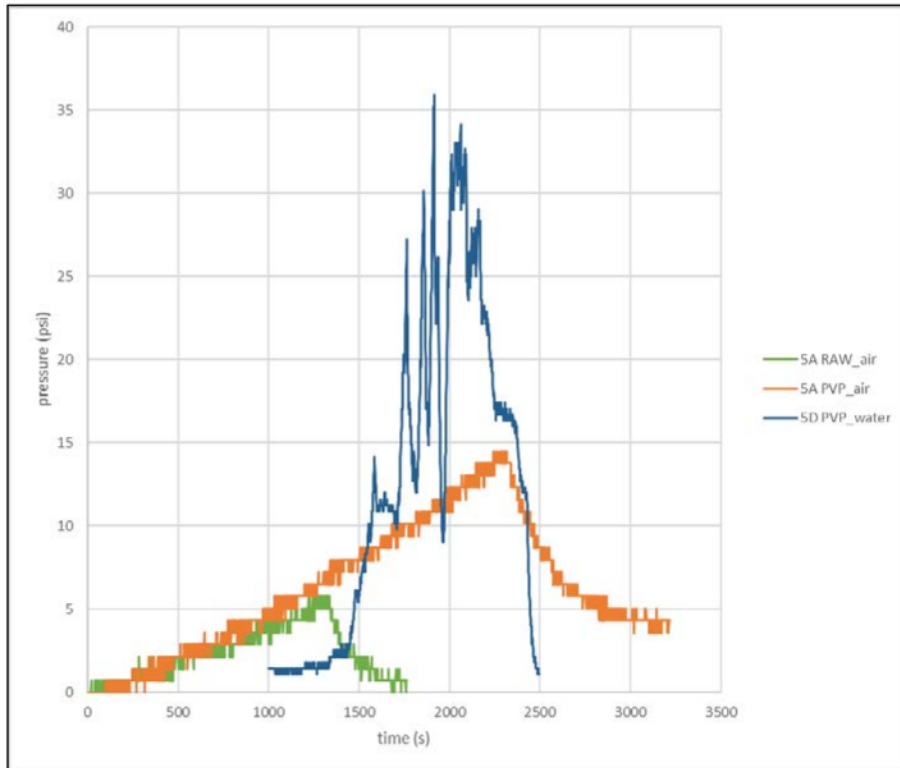


Figure 28: Third and fourth hydraulic test. Five 3.5" plugs (5A raw / 5A PVP) installed in 1m of 4" pipe are tested after 48 days of hydration using a constant pump rate of 2.4l/h (0.7ml/s). The blue curve in the background represents 1m equivalent of 5D PVP tested after 51 days using water.



Figure 29: 5A-PVP in a 4" pipe/ third hydraulic test. Air bubbles occur at the interface plug/steel pipe at failure pressure.



Figure 30: 5A-raw in a 4" pipe / fourth hydraulic test. Air bubbles occur at the center of the plug and at the interface plug/steel pipe at failure pressure.

6 Hydraulic long-term testing of the most promising materials

The two most promising bentonite materials to be tested in the long term test program are the 5D and the 5A bentonite of Amcol Australia Pty Ltd, as shown in the Section 2.2 and Chapter 5. Pre-hydrated plugs in single pipe sections were prepared and stored with a PVC pipe extension on top of the pipe to guarantee a continuous hydraulic head on top of the plugged section. The total number of tests was limited by the amount of pipe segments available. The 4" pipes, loaded with 3.5" plugs of 5D PVP and 5A PVP were chosen for a testing program including three measurements per material, after each 3, 6 and 9 month hydration time. A 4m high 6" pipe section was loaded with seventeen 5" plugs of 5D PVP as a permanent setup, which was tested after 2, 4, 6 and 8 months of hydration. This experimental design was also chosen to test the re-healing performance of already dislodged bentonite plug sections. This test is ongoing and the plugged section will stay installed on the Well Simulator Facility beyond the end of the project for further long-term testing. The 8" pipes were loaded with 5.5" plugs of the 5D PVP material. A sandstone cylinder was installed in an 8" steel pipe to simulate open hole conditions at the Well Simulator Facility.

The results of the hydraulic long-term testing series are summarized in Section 6.5.

6.1 Results of the 4" pipe sections

Three 4" pipe sections were loaded with five 5A PVP and 5D PVP bentonite plugs each and pre hydrated in the laboratory. The results of the six hydraulic tests of the 4" pipe long term testing are shown in Figure 31. The samples were tested after hydrating for 99, 183, and 296 days. After all three tests the 5D PVP bentonite performed significantly better than the 5A PVP. The failure pressure of 5D PVP is nearly double as high after 296 days as the one from the 5A material. Water production on top of the plugged sections could be detected in all tests.

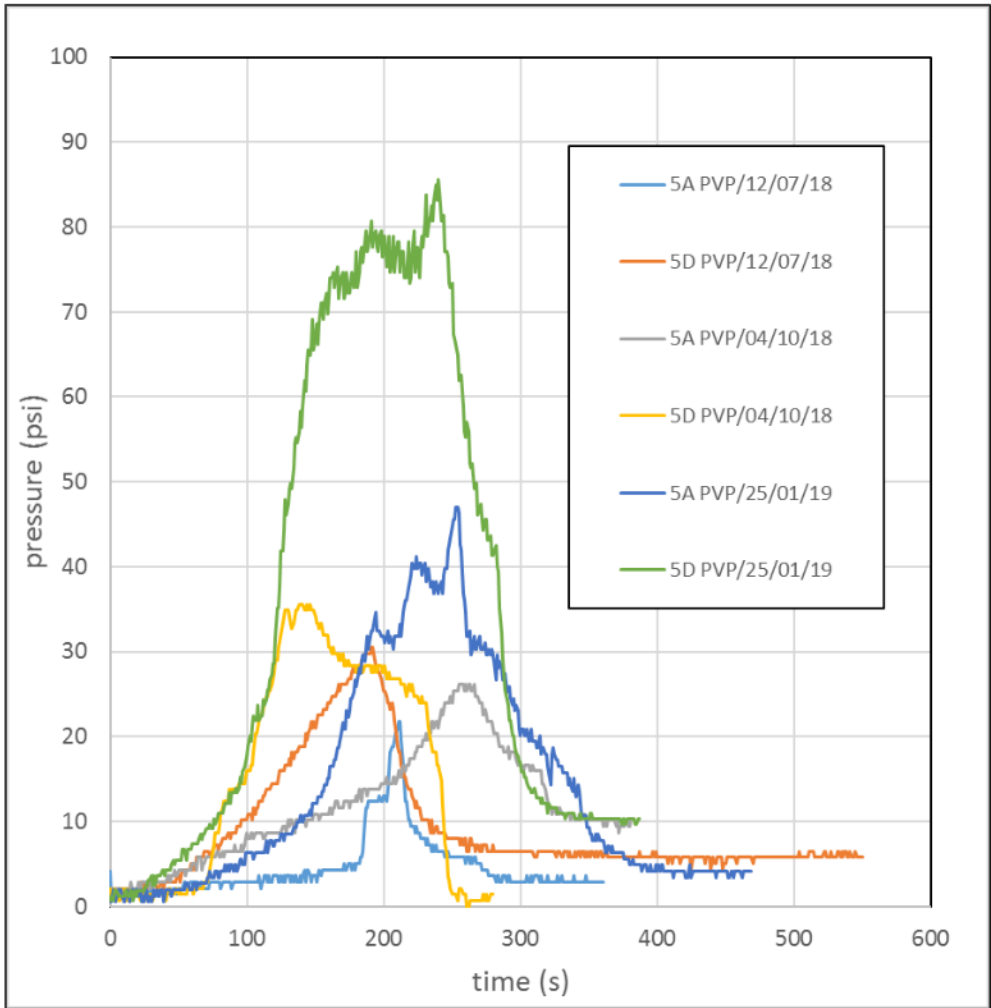


Figure 31: The six hydraulic tests of the 4" long term testing series: Five 3.5" plugs (5D PVP/5A PVP) installed in 1m of 4" pipe are tested after 99, 183 and 296 days of pre-hydration using a constant pump rate of 2.4l/h (0.7ml/s).

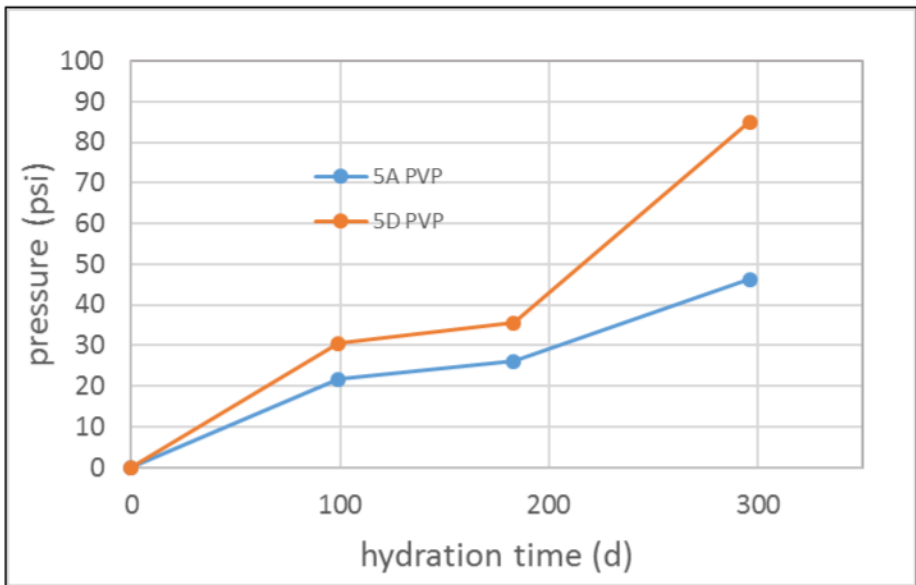


Figure 32: Time dependent failure pressures of 1m high 4" pipe sections filled with hydrated 5A PVP and 5D PVP bentonite. The 5D PVP material shows significantly higher pressures than the 5A Bentonite

6.2 Results of the 6" pipe sections

5" diameter plugs were prepared by stripping 0.5" from the originally produced 5.5" plugs (Figure 33). A section of 4m was filled with the plugs and hydrated. Water was refilled weekly at the top to assure a constant water head on the installed bentonite. This experiment was designed for two purposes: to test the long term failure behavior of the plugs and to examine the "self-healing" ability of the plugged section after being dislodged (Towler et al. 2015). It was expected that the sealing performance of the bentonite plug during/after the healing process would actually increase.



Figure 33: Originally, 5.5" diameter plug, stripped to 5" for the long term 6" pipe section testing.

The pump rates were increased during the third and fourth test, because no water production could be detected at the top of the plugged section after the first pressure drops (black arrows in the Figure 34). The massive increase of pressure at final failure seems to be impacted by the "shear-thickening" effect of non-Newtonian fluids as already described in Chapter 6.

Figure 35 shows two curves, representing the pressures at maximum failure pressure (5D PVP) and the pressure readings after the first pressure drops at constant flow rate (5D PVP / alternative interpretation). The 5D PVP readings of the third and fourth tests are most likely as high because of the pump rate triggered effect mentioned above and should be disregarded.

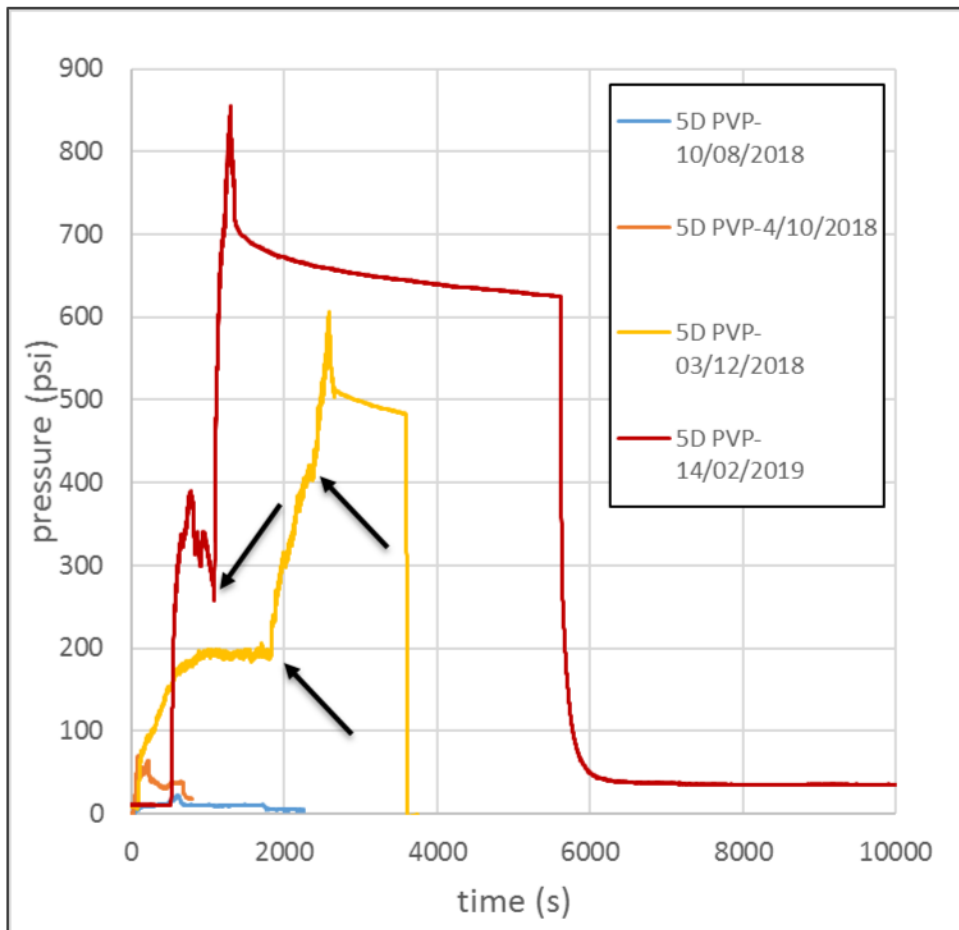


Figure 34: The four hydraulic tests of the 6" long term testing series: seventeen 5" plugs (5D PVP) installed in 4m of 6" pipe are tested after 65, 120, 148 and 253 days of hydration using a constant pump rate of 2.4l/h (0.7ml/s) during the first two tests. The pump rates were increased during the third and fourth test, because no water production could be detected after the first pressure drops (arrows in the graph).

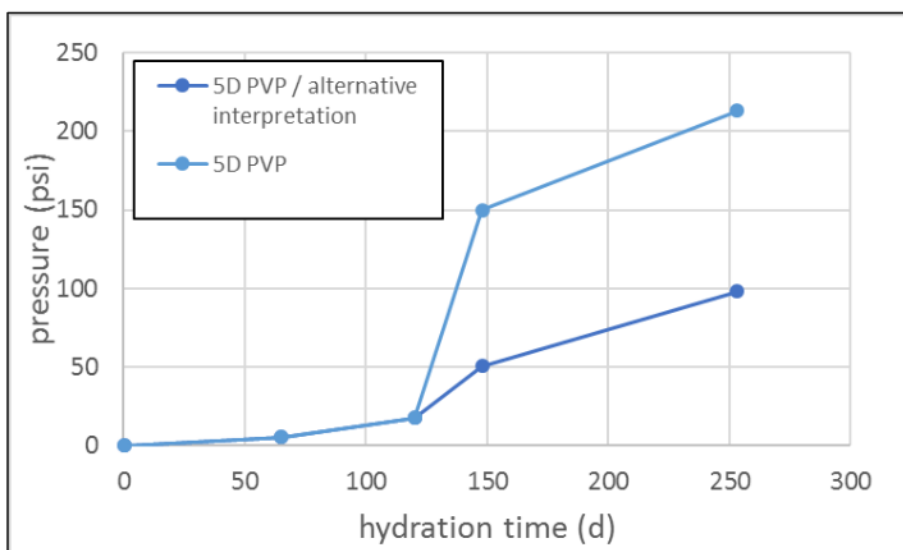


Figure 35: Time dependent failure pressures of a 1m high pipe section filled with hydrated 5D PVP bentonite. The original data were height converted for better comparability with the long term 4" test results.

6.3 Results of the 8" pipe sections

A 1m plugged section of 5.5" plugs was installed in an 8" pipe and tested after 85 days of hydration, using a constant pump rate of 2.4l/h (0.7ml/s). Final failure pressure was measured to be 10.2psi after

545 seconds of flow when water production was detected on top of the plugged section (Figure 36). The hydrated plugs slipped out of the casing when the pipe was removed from the rig. This is an example for the limitations of the bentonite plugging technology as it stands at the time of the reporting. The 5.5" plugs were not able to expand enough to create a proper seal in the 8" pipe section.

We decided not to proceed with the 8" testing geometry because the moisture content of the hydrated plug was simply too high to create a proper seal.

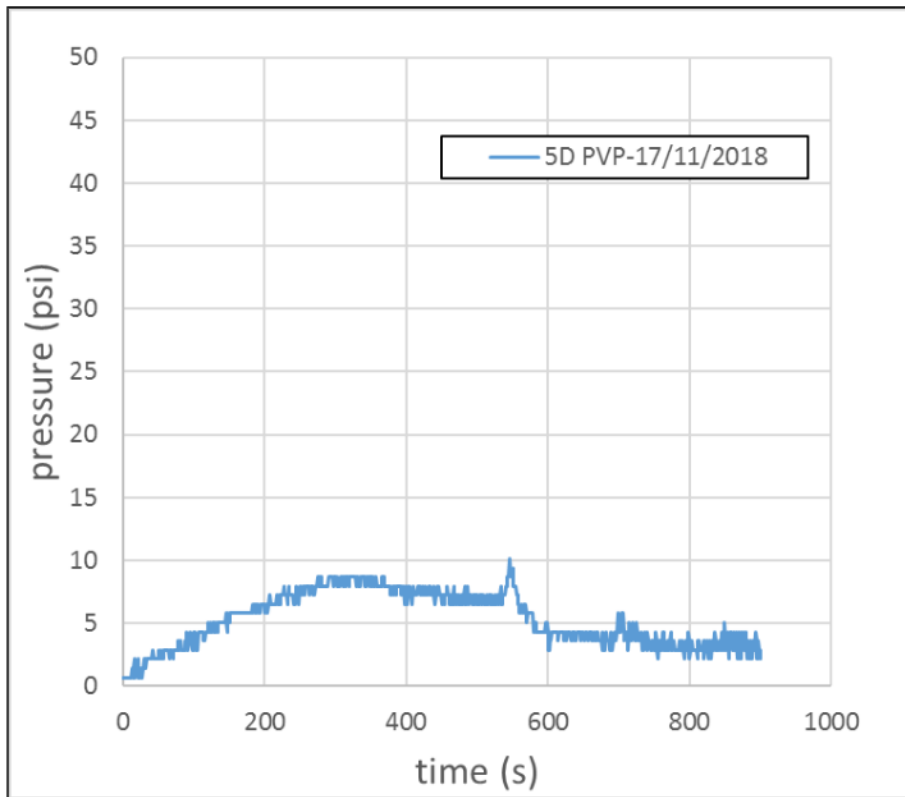


Figure 36: 1m plugged section / 5.5" plugs in 8" pipe / 5D PVP, tested after 85 days of hydration using a constant pump rate of 2.4l/h (0.7ml/s).

6.4 Simulation of testing of bentonite plugs in uncased holes

An 80cm long sandstone cylinder with an ID of 94 mm was drilled out of a block of Helidon Sandstone out of the Ipswich-Moreton Basin (Figure 37 and Figure 38). This geometry is close to HQ size (96mm), which is the usual size of continuously cored boreholes in the coal exploration industry in Queensland. The sandstone pipe was glued into one of the 8" steel casings of the Well Simulator Facility, using a high tensile and flexural strength, low viscosity epoxy resin (Sikadur-52) to mimic open hole conditions (Figure 39). The Helidon Sandstone is an equivalent to the Lower Jurassic Precipice Sandstone, which is the basal sedimentary deposit within the Surat Basin succession. This was the only trial using a natural rock as containment for the hydrated plugs in the Well Simulator. Different lithologies like claystones or even coal would be desirable to cover most of the existing rock types in the Surat Basin. Unfortunately, they would not survive primary drilling, the gluing process and finally the hydraulic test program, because of their swelling abilities and brittle failure behaviour.



Figure 37: 80cm log Helidon Sandstone cylinder.



Figure 38: Helidon Sandstone Cylinder (94mm ID).



Figure 39: Helidon Sandstone Cylinder after hydraulic testing. The sandstone is installed in an 8" steel casing, using a high tensile and flexural strength, low viscosity epoxy resin.

The cylinder was loaded with four 19cm high 3" 5D PVP bentonite plugs (stripped down from 3.5" originally plug size). It was tested after 98, 122 and 146 days of hydration. The results of the hydraulic tests are shown in Figure 40. A constant pump rate of 2.4l/h (0.7ml/s) was used for sample 17-07-water (grey curve) and the maximum failure pressure reading was 122.5psi when water production was detected on top of the plug. Samples 10-08-water and 03-09-water did not show water production after reaching an average plateau pressure. The decision was made to double the pump rate for sample 10-08-water and the final failure seems to be impacted again by the "shear-thickening" effect of non-Newtonian fluids as described in Chapter 6. The pump rate was only increased to 2.8l/h (0.8ml/s) for sample 03-09-water, which triggered immediate failure after a small pressure increase of 15psi, showing a sharp pressure peak in the blue curve. The average pressures before failure were used for the failure pressure comparison because of the flow rate variations at the end of the two later tests. The presented failure pressures are measured using the 0.8m plugged section (Figure 40), but later converted to a 1m plugged section to make them comparable to the other presented failure pressure results (Figure 41 and Section 6.5). The failure pressures are substantially higher than in comparable plug/pipe ratio sizes. This is most likely caused by the roughness of the sandstone cylinder surface. Higher frictional forces have to be overcome to create failure of the bentonite plugged section in the sandstone compared to a plugged section in a steel casing with relatively smooth surface.

This result has also important implication for the design of abandonment operations of older wells with significant casing corrosion. Corroded steel pipes with rough surfaces will withstand significantly higher pressures while plugged with bentonite than new casings. We can't quantify this effect to date. Research on the influence of surface roughness to failure pressures of bentonite plugs was not manageable within the limited timeframe of the project, but might become a focal point for a

successor project.

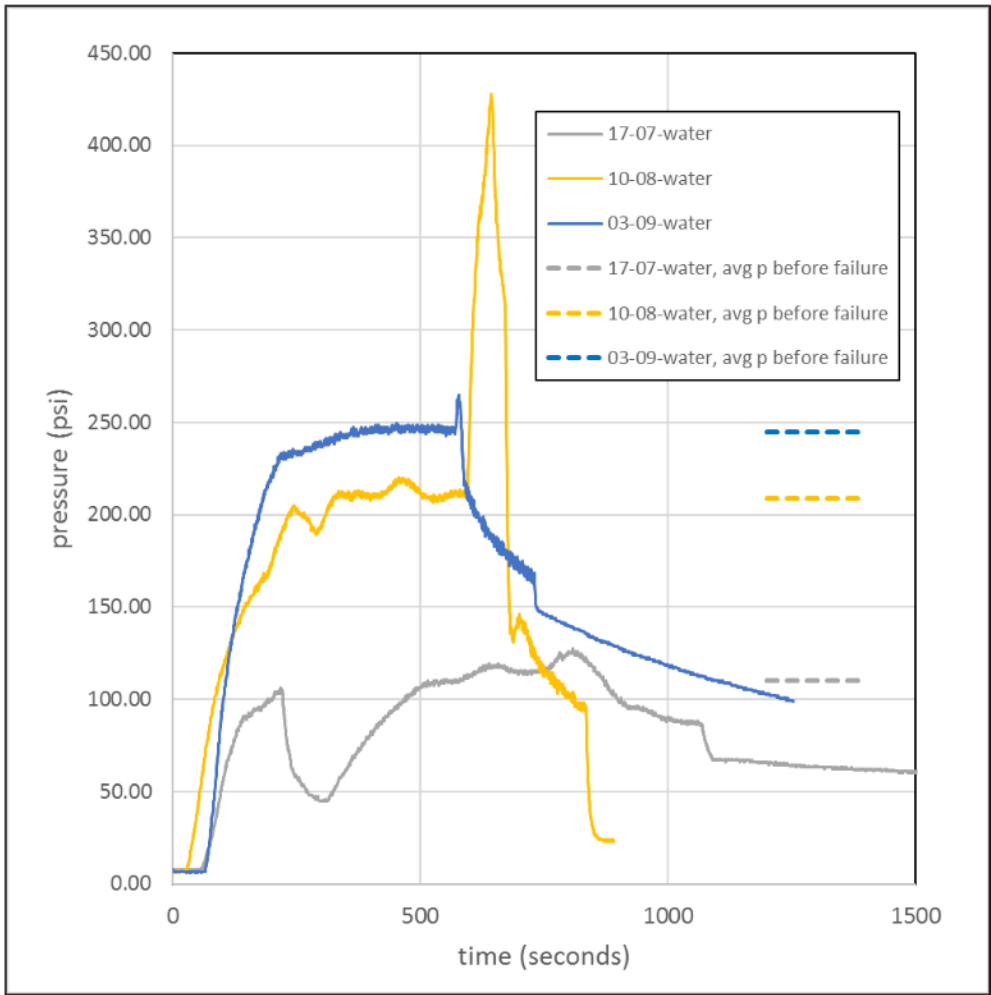


Figure 40: The three hydraulic tests of the Helidon Sandstone cylinder installed in an 8" steel pipe: four 19cm high 3" 5D PVP bentonite plugs (stripped down from 3.5" originally plug size) were hydrated and tested in two month intervals using a constant pump rate of 2.4l/h (0.7ml/s). The presented failure pressures are measured for the 0.8m plugged section.

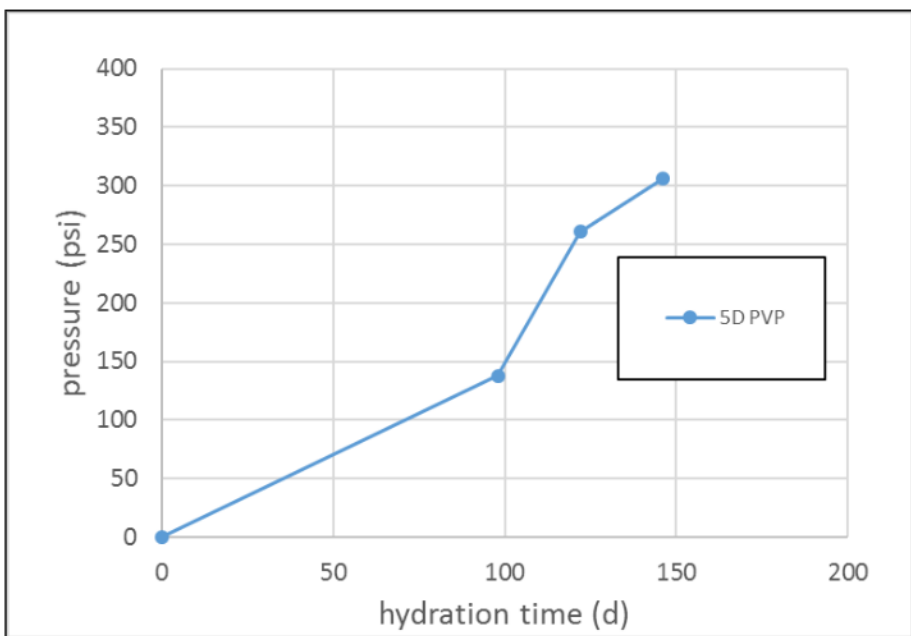


Figure 41: Time dependent average failure pressures of a 1m high sandstone cylinder section filled with hydrated 5D PVP

bentonite. The average failure pressures are converted to a 1m plugged section to make them comparable to the other presented failure pressure results.

6.5 Summary of the results of the hydraulic long term testing

A summary of the failure pressures of all long term hydraulic test results is given in Table 8 and Figure 42. The erroneous results of the experiment 6" 5D PVP (highlighted) are included in the table and the figure beside the alternative interpretation (6" alternative 5D PVP) which is not impacted by the "shear-thickening" effect of non-Newtonian fluids as described in Chapter 6.

4" 5A PVP		failure pressure (psi)	failure pressure (bar)	days of hydration	failure gradient (psi/ft)	failure gradient (bar/m)
test	date					
start	5/04/2018	0	0	0	0	0
1st	12/07/2018	21.8	1.5	99	6.6	1.5
2nd	4/10/2018	26.1	1.8	183	8.0	1.8
3rd	25/01/2019	46.3	3.2	296	14.1	3.2

4" 5D PVP		failure pressure (psi)	failure pressure (bar)	days of hydration	failure gradient (psi/ft)	failure gradient (bar/m)
test	date					
start	5/04/2018	0	0	0	0	0
1st	12/07/2018	30.5	2.1	99	9.3	2.1
2nd	4/10/2018	35.6	2.5	183	10.8	2.5
3rd	25/01/2019	85	5.9	296	25.9	5.9

6" 5D PVP		failure pressure (psi)	failure pressure (bar)	days of hydration	failure gradient (psi/ft)	failure gradient (bar/m)
test	date					
start	7/06/2018	0	0	0	0	0
1st	10/08/2018	5.5	0.4	65	1.7	0.4
2nd	4/10/2018	17.6	1.2	120	5.4	1.2
3rd	1/11/2018	150.1	10.3	148	45.8	10.3
4th	14/02/2019	213.1	14.7	253	65	14.7

6" alternative 5D PVP		failure pressure (psi)	failure pressure (bar)	days of hydration	failure gradient (psi/ft)	failure gradient (bar/m)
test	date					
start	7/06/2018	0	0	0	0	0
1st	10/08/2018	5.5	0.4	65	1.7	0.4
2nd	4/10/2018	17.6	1.2	120	5.4	1.2
3rd	1/11/2018	50.5	3.5	148	15.4	3.5
4th	14/02/2019	98	6.8	253	29.9	6.8

8" 5D PVP		failure pressure (psi)	failure pressure (bar)	days of hydration	failure gradient (psi/ft)	failure gradient (bar/m)
test	date					
start	25/08/2017	0	0	0	0	0
1st	17/11/2017	10.2	0.7	85	3.1	0.7

sst. tube 5D PVP		failure pressure (psi)	failure pressure (bar)	days of hydration	failure gradient (psi/ft)	failure gradient (bar/m)
test	date					
start	10/04/2018	0	0	0	0	0
1st	17/07/2018	138	9.5	98	42.1	9.5
2nd	10/08/2018	261	18.0	122	79.6	18.0
3rd	3/09/2018	306	21.1	146	93.3	21.1

Table 8: Summary of all long term hydraulic test results commenced during the project time.

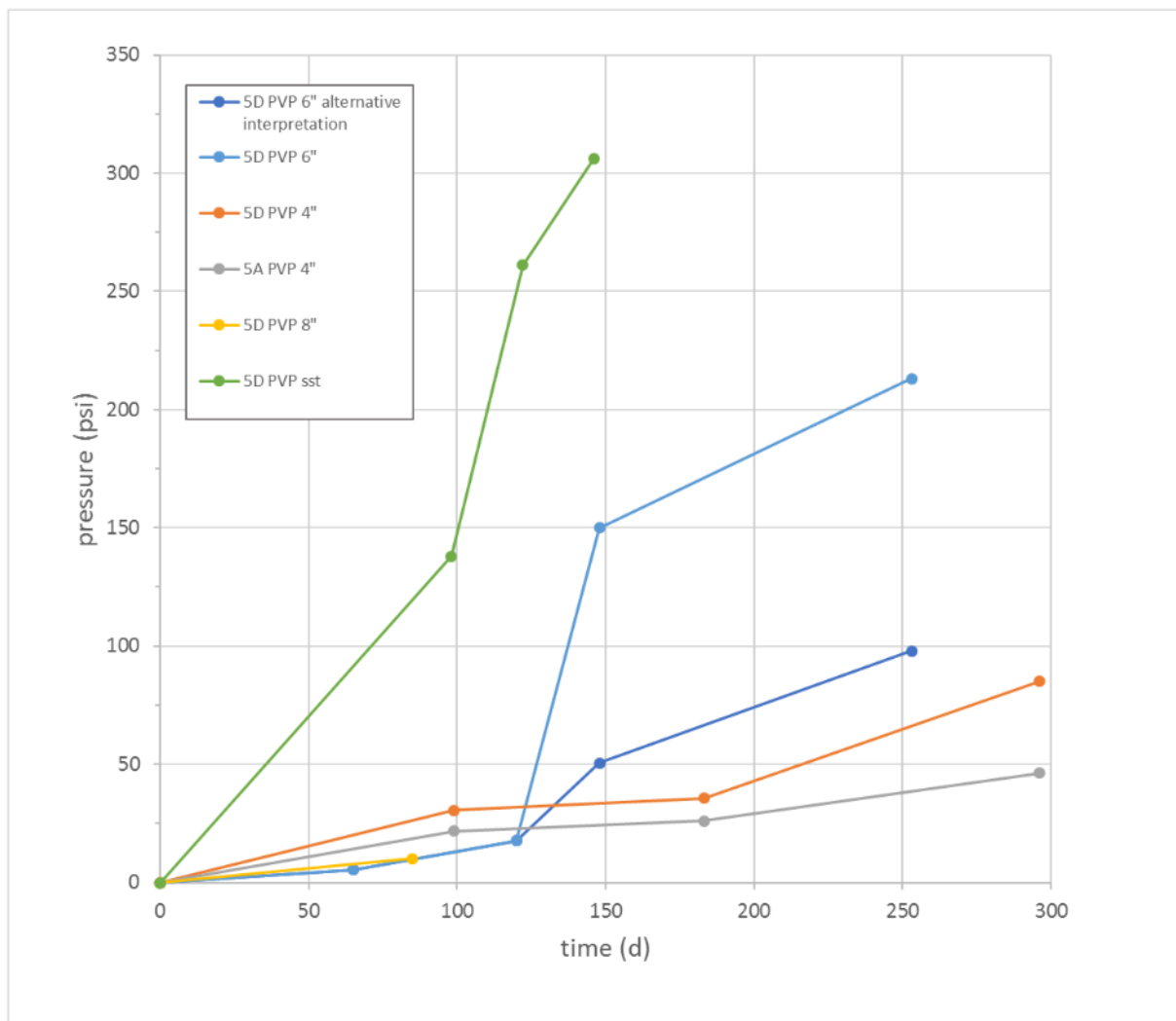


Figure 42: Summary of all time dependent failure pressures of 1m high plugged sections of the hydraulic long term tests. The bright blue line shows the erroneous results of the experiment impacted by the “shear-thickening” effect of non-Newtonian fluids as described in Chapter 6. The dark blue line represents pressures derived using a constant pump rate.

The comparison of the two best performing bentonite materials show a clear result: the best performing material is the 5D PVP blend that is able to hold pressure gradients up to 25.9 psi/ft or 5.9 bar/m (Table 9) after 296 days of hydration. The results of the 6” testing are not as conclusive. Figure 42 show two blue curves for the 6” 5D PVP plugs: The bright blue curve with the abnormally high pressure readings for the two last data points caused by the “shear-thickening” effect triggered by increased pump rates and the dark blue curve (alternative interpretation) representing failure after using constant pump rate of 2.4l/h (0.7ml/s).

It was expected that the dark blue curve would plot below the grey curve representing a pipe/plug combination with a smaller diameter. Bentonite is more stable in its plugging performance if it has to fill smaller “voids” after hydration (see Section 6.3) which is directly related to the in situ moisture content (Towler et al., in prep.). The higher the final moisture content, the weaker the plugged section. The increased pressure volumes of the two last readings of the dark blue curve (alternative interpretation) are well above the 4” results. This is caused by re-healing of the bentonite plugged section. The plug is increasing in strength after being disturbed due to the testing and later rehydration (Towler et al., in prep.).

The most surprising result is the performance of the 5D PVP blend in the open hole simulation. The

influence of high frictional forces associated with the rough surface area of the sandstone cylinder seems to be the dominant factor influencing the final failure. More research is needed to explain the observed high failure pressure gradient of this specific experiment.

The failure gradients shown in Table 9 can be used for the design of abandonment operations using comparable plug/pipe diameters. The 5D PVP blend is easily able to withstand 1000psi reservoir pressure in a 4" casing after installing a 30m plugged section, even after reducing the reported gradient by a 50% safety/contingency margin for the basis of design.

	failure gradient	failure gradient	failure pressure for a 30m plugged section	
	(psi/ft)	(bar/m)	(psi)	(bar)
4" 5A PVP	14.1	3.2	1389	96
4" 5D PVP	25.9	5.9	2549	176
6" 5D PVP	65.0	14.7	6396	1763
6" alt. 5D PVP	29.9	6.8	2959	811
8" 5D PVP	3.1	0.7	306	21
sst. 5D PVP	93.3	21.1	9180	633

Table 9: Failure gradients for all tested plug/pipe combinations. 30 m of plugged pipe section is a standard height for abandonment operations in the drilling industry using cement. The orange highlighted line shows the erroneous results of the experiment impacted again by the “shear-thickening” effect of non-Newtonian fluids as described in Chapter 6.

7 “Pumpable solution”

The industry partners of UQ CCSG and representatives from Department of Natural Resources, Mines and Energy (DNRME) suggested the project develop and test a “pumpable solution” of the bentonite technology. Background for this approach is the need to place cement through perforated liners to fill the voids between liner and rock. A pumpable bentonite slurry mostly consists of dispersed montmorillonite particles, which are not able to expand any further. Mixing up to 3% bentonite into cement is a commonly used practice to lubricate the material and to reduce the required horsepower of pumping equipment. We explored this concept by using a grout as lubricant to pump one metre sections of small compressed bentonite cylinders and 0.25” bentonite tablets through a translucent PVC hose. Pump trials were commenced in November 2018.

20m of 2 and 2.5” ID translucent reinforced PVC hoses were used for the pumping experiments (Figure 43). Pressure limitations for the 2”ID hose were 205psi working pressure and 610psi bursting pressure at 23°C, and for the 2.5” hose 175psi WP and 520psi BP at 23°C.

The shrinking compensated grout used for lubrication of the compressed bentonite was NaX™ WP 19 provided by Nautec Australia (technical data: Appendix 11). The 0.25” uncoated bentonite tablets (CETCO® TABLETS) were provided by Cetco Drilling Products Australia (technical data: Appendix 12).

5D PVP blend was used to compact the 2” diameter cylindrical plugs with a height of 10cm (Figure 44) using an industrial hydraulic press applying 15t. Ten of these plugs were fed into a 10m long 2.5” hose (Figure 45) after preloading a foam cylinder, which is usually used to clean out cement hoses. Grout was added afterwards as a lubricant during the pumping process. Finally another foam cylinder was loaded to separate the bentonite plugs and the grout from the water we used for pumping. This process was repeated with the 2” hose, loading bentonite tablets (Figure 46) and the same grout, again separated from the water with foam cylinders.

Water lines with 70 and 140 psi were available in the laboratory of the School of Chemical Engineering to commence the pump trials. 70psi was sufficient to pump the 1m long plugged section through the whole length of the horizontally arranged hoses reaching a speed of approximately 1m/10s. The water was shut down after pumping the plugs to the end of the hoses and the sample were shut in for a 65-day hydrating/curing period.

The 1m plugged section were tested after 65 days using the 140psi water line. The hoses were pressured up and the pressure was held for four hours for both tests. The hose section behind the plugs were opened to detect water flow in case of failure. Both bentonite grout blends were able to hold the 140psi pressure for four hours with no water flow detected.

This experiment indicates that placement of compressed bentonite in conjunction with grout lubrication is even possible in horizontal well sections using common pumping technology in combination with poly pipe or metal coiled tubing technology.



Figure 43: 20m sections of 2 and 2.5" ID translucent reinforced PVC hoses used for the pumping trials.



Figure 44: 2" diameter cylindrical plugs with a height of 10cm, compressed with 15t.



Figure 45: Placing of ten plugs into a 10m long 2.5" hose.



Figure 46: Loading compressed bentonite tablets into a 10m long 2" hose.

8 Field trials

8.1 Bellevue #GW3 (Shell/QGC)

The Bellevue #GW3 (Shell/QGC) field trial was completed before the start of the AQIP program on March 8, 2017. It is reported here to give a comprehensive overview about all abandonment field trials using bentonite plugs.

The Bellevue #GW3 P&A operations are described in detail in the presentation given at the Technical Work Group meeting on the 23/08/2016 (Holl 2016—see Appendix 13).

Abandonment operations were commenced on 27/07/2016 (Appendix 14). Five plugs were dropped at 30 second intervals after circulating the well to fresh water and a 60 minute flow check. Tagging with CT indicated that the plugs were placed at expected depth.

At the 28/07/2016 two batches of 100 plugs each were dropped successfully at 10 second intervals and tagged at expected depth. After dropping the first two batches successfully it was decided to increase the number of plugs to be dropped before tagging to 200. Bridging of the bentonite plugs was identified after dropping 176 plugs. The plugs turned up at surface and could have create a bridge of a maximum of 42.24 mGL (metres below ground level) if a homogeneous bridge including all 176 plugs had formed. Trials to push the bridge down using the CT and the use of a jetting tool to wash out the plugs were unsuccessful.

Two bridged sections were drilled out on 29/07/2016 using a 3 ¾" mudmotor with a 6 ⅛" tricone bit and the top of the actual plug was tagged as before (at the top of the second batch of 100 plugs).

A scraper was run early next morning (30/07/2016) to clean the casing above the plug. It was decided

to go back to groups of 50 plugs to be dropped and tagging after placing each batch.

A possible reason for bridging off might be the damage of some plugs during the manual dropping process as a couple of plugs knocked on the sharp edges of the thread inside the 7" casing collar while dropping. These plugs are believed to have broken on their way down the hole, tilted after a while and got stuck, finally creating the bridges. After this event additional training of the crew was arranged ensuring that plugs were dropped in the centre of the bore, avoiding any contact with the casing collar thread.

443 plugs were dropped successfully on 30/07/2016. The uppermost plug was tagged at a depth of 29.57 mGL.

On 31/07/2016 a further 77 plugs were dropped and tagged at a depth of 12 mGL as per the approved abandonment program. The well was then topped up with fresh water and a 7" swage with a 2" ball valve was installed.

Pressure testing was commenced on 30/09/2016, 4 weeks after the P&A operations. The bentonite plug was pressure tested to 250 psi for 5 minutes followed by 500 psi for 60 minutes. The pressure was observed to be holding through the duration of the test. Zero pressure reduction or leakage was noted from the pressure profile.

The pressure test was successfully repeated at the 06/02/2017 and the results were reported to the regulator (250psi for 5 minutes and 500psi for 35 minutes).

This was the first time bentonite plugs were used successfully to plug and abandon a water monitoring well in an operating CSG field in Queensland.

8.2 Coal exploration well R 2315 (DNRME)

DNRME offered UQ CCSG a legacy coal exploration bore 15km WSW of Chinchilla for the purpose of a field trial of the bentonite plugging technology in conjunction with a shrinkage compensated grout developed by Nautec. Records show the bore to have a nominal diameter 4 ¾" (121mm), was drilled with a blade bit in 1981 and has a nominal depth of 114 mGL, exposing a sequence of some 13 potential coal seams. The bore had no reported casing or collar in place and there was no record of abandonment operations or of a protective cover plate. The most likely position of the well was marked by a star picket, covered by a free standing PVC pipe. Gas monitoring during the first visit showed a consistent presence of methane in the atmosphere. 10% LEL was measured with a handheld device three metres from the PVC pipe. A maximum level of 27% LEL was measured on a piece of tree bark at 1.5m distance from the star picket (Fig.1, Appendix 18). It was concluded that methane gas was migrating to the surface via a poorly abandoned well (Appendix 15).

The trial was carried out in October 2018, with a Nautec grout installed between 113.7 m to 94.7 mGL and the bentonite plugs between 94.7m and 6 mGL . 467 bentonite plugs were placed successfully on top of the grout to reach the final top of the plugged section at 6 mGL. The well was than filled up with water and a lockable lid with a ½" outlet was installed on the 7" conductor pipe to allow periodical gas monitoring. A summary of the results of methane gas concentration measurements before, during and after abandonment operations is shown in Figure 47.

Abandonment operations are reported in detail in Appendix 15, an overview of the operations is given in the attached presentation (Appendix 16), and a poster presented at the UQ Research Review 2018

(Appendix 17). A major learning point of the field trial was the successful application of nylon spacers to pump remaining bentonite out of the HWT pipe, which was used to deploy the plugs in the open hole. The spacers were used to clean up the pipe after bridging events during the plug placement. Bridging of plugs was a major problem during the abandonment operations at the Bellevue #GW3 field trial (see Section 8.1). We are planning to use grout to create this spacer geometry for future abandonment operations.

DNRME planned to continue the gas monitoring of the well for six months following installation to assess the trial’s effectiveness (see Section 8.2.1). UQ CCSG did additional gas surveys in the surrounding area and at the well location (see Section 8.2.2).

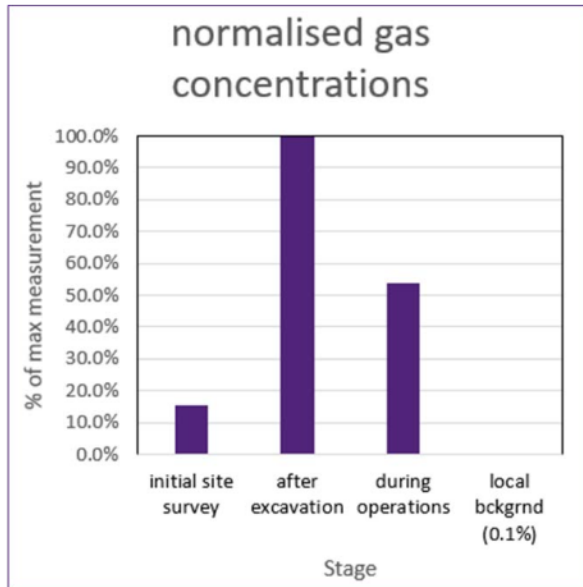


Figure 47: Normalised gas concentrations at the R2315 well site before, during and after abandonment operations.

8.2.1 DNRME methane surveys

The post plug and abandonment operations gas measurements commenced by DNRME are reported in Appendix 18. A Handheld Laser Methane mini (LMm) detector was used for this survey (technical specifications are in the appendix). Measurements were done around the lockable well lid and in the surrounding are of R2315 along Greenswamp Road (compare maps in Appendix 18).

8.2.2 UQ Greenswamp Road coalhole and atmospheric methane surveys (by Dr Des Owen, CCSG)

A series of free gas sampling and surveys were performed at a number of sites along Greenswamp Road Chinchilla to assess the discharge of methane from coalholes, and the potential for other point-sources of methane to occur in the area. This included:

1. Sampling of free gas discharging from an open coalhole on Greenswamp Road, R2315, and analysis of gas composition and isotope composition of methane gas – 3/10/2018.
2. Methane gas surveys using a laser methane meter at the following sites: i) R2315 and another unnamed coalhole on Greenswamp Road; and ii) along particular transects of Greenswamp Road.
3. Methane gas flux measurements from particular sites detected in the methane gas surveys.
4. Hydrocarbon and other gas capture at R2315 and another open coalhole on Greenswamp Road using suma cannisters (a type of gas bottle that captures atmospheric gas over time).

8.2.2.1 Sampling free gas from R2315

The open coalhole R2315 was identified discharging methane gas to the atmosphere. This coalhole had collapsed at an unknown depth. A 125mm PVC pipe casing was installed by DNRME to a depth of 400 mm. The PVC casing was partially filled with soil, and extended 1130 mm above the ground surface. The internal height from soil within the PVC casing to the top of the PVC pipe was 1500mm (Figure 48). To sample methane degassing from the hole, a sealed PVC housing was attached to the open end of the PVC casing. This PVC housing extended the PVC casing by approximately 800 mm. The total internal PVC headspace volume with the PVC housing attached was approximately 28 litres. The PVC housing contained two manual valves: one to allow vacuum purging of the headspace, and another to allow gas sampling. A 3 litre manual vacuum pump was used to pump 30 litres from the PVC headspace (purging). Care was taken not to “over-purge” the headspace, which would increase the risk of drawing atmospheric and/or soil gases into the headspace. Following purging, three free gas sampling events, with two replicates, were taken via the sampling valve using an IsoBag® manual hand pump at 10 minute intervals (total samples n = 6).

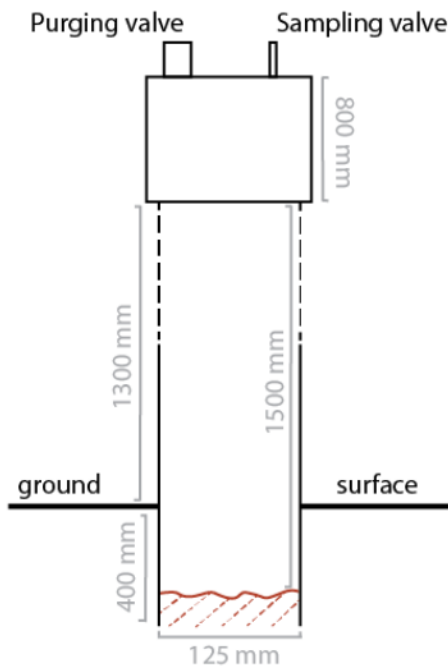


Figure 48: Conceptual diagram of the PVC housing and valve arrangement at R2315 (not to scale).

The methane concentration of gas samples taken from R2315 ranged from 119,184 – 211,206 ppm/volume (ppm/v). Figure 49 shows that over the sampling period (30 minutes) the methane concentration of gas in the PVC housing approximately doubled. High ppm/v concentrations, 119,184 ppm/v and 121,159 ppm/v, for the samples taken after 10 minutes indicate that the flux of methane from coalhole, through the soil, into the PVC housing was high and rapid. Background atmospheric methane in the Surat Basin is not well documented prior to coal exploration in the 1980s, but for comparison the ambient methane concentration at a global monitoring station at Cape Grim, Tasmania, is ~1.8 ppm/v (Stalker 2013). The rapid discharge of methane was also visually evident by an opaque gas plume exiting the purging valve prior to purging. Increases in the methane ppm/v over the sampling period indicate ongoing methane flux; however, it was not possible to determine flux (mass per unit area of time) with the equipment installed on site. Nonetheless, the results indicate the presence of a point-source methane plume continually discharging from the abandoned coalhole R2315.

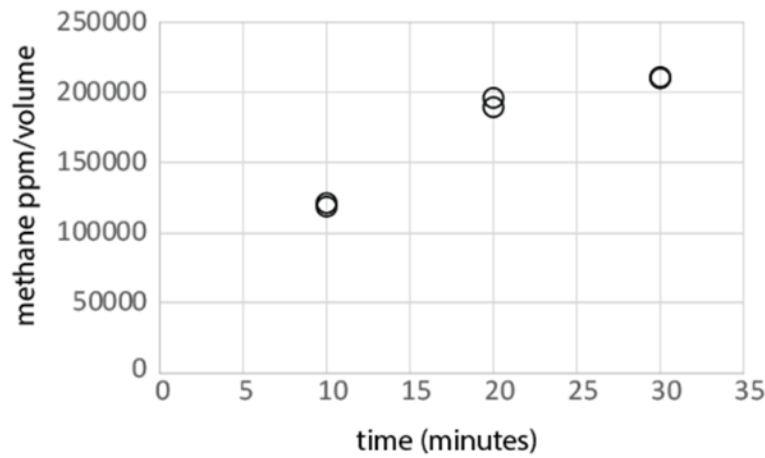


Figure 49: Methane concentrations (ppm/v) sampled from the PVC housing over time.

Free gas samples were also analysed for the stable carbon and hydrogen isotopes of methane, $\delta^{13}\text{C}-\text{CH}_4$ and $\delta^2\text{H}-\text{CH}_4$, respectively. The measured $\delta^{13}\text{C}-\text{CH}_4$ and $\delta^2\text{H}-\text{CH}_4$ values for all samples ranged from -63‰ to -62.1‰ and -227‰ to -223‰, respectively (Figure 50). These values are within the range of previously measured stable carbon and hydrogen isotopes of biogenic methane in the Surat Basin, but are relatively depleted when compared to $\delta^{13}\text{C}-\text{CH}_4$ from commercial biogenic CSG reservoirs in the basin (Draper & Boreham 2006, Golding et al. 2013, Hamilton et al. 2014, Baublys et al. 2015, Owen et al. 2016). These depleted values of $\delta^{13}\text{C}-\text{CH}_4$ are similar to measured $\delta^{13}\text{C}-\text{CH}_4$ of dissolved methane from shallow (<200 m) areas of the Walloon Coal Measures (Owen et al. 2016), indicating the gas source at this abandoned coalhole is likely a shallow gas source, and not related to deeper CSG reservoirs. While isotope data from shallow Walloon Coal Measures and other overlying formations in the Surat is limited, compared to isotopic data from the CSG reservoirs, a small gas kick during drilling at 23 m also suggests that the methane is derived from a shallow gas source.

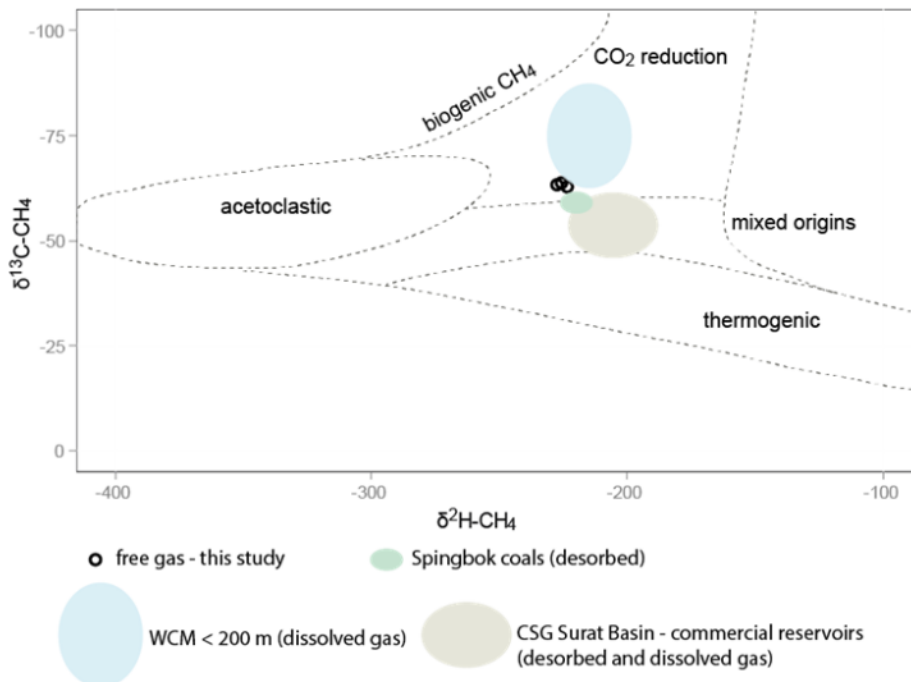


Figure 50: Measured $\delta^{13}\text{C}-\text{CH}_4$ and $\delta^2\text{H}-\text{CH}_4$ values from free gas samples taken during this study. Shaded areas representing comparative ranges of measured isotope values from: shallow (<200 m) Walloon Coal Measures (Owen et al., 2016); Springbok coals (Hamilton et al., 2014); and CSG from commercial reservoirs (Draper and Boreham, 2006; Golding et al., 2013; Hamilton et al., 2014; Baublys et al., 2015).

8.2.2.2 Methane gas surveys – Greenswamp Road

This survey was originally commenced by the “Shallow Gas Project”, UQ CCSG to identify and measure methane migration on top of a seismically identified anomaly. The gas surveys consisted of two sequential methane gas survey techniques at both the seismic anomaly site and the control site:

1. Gas plume detection conducted via methane gas scanning surveys using a prototype laser detector via traversing a specific section of Greenswamp Road and a nearby road, Nothdurfts Road, in a vehicle travelling ~10-15 km/h. Nothdurft Road survey provides a local comparison/control site relative to the Green; and
2. At specific locations where methane gas plumes were identified in step 1, flux hoods coupled to gas to determine the flux of methane over time and the concentration of different gases, respectively.
3. Collection of atmospheric and soil gases over time using summa canisters (a type of gas canister) to determine gas composition in specific areas.

The methane gas surveys were conducted by Terra Sana Consultants Pty Ltd on 11 December 2018, and details of these surveys included in this report are derived from a report provided by Terra Sana to UQ on 12th February 2019.

Laser Methane detector surveys

Laser methane detector data was collected using prototype open-path absorption spectroscopy detector (detection limit 1 ppm/m, detection speed 0.1 s, detection distance 0.5-100 metres) coupled with a real-time data acquisition system.

Laser methane sensors work by emitting a laser beam with a specific wavelength, and then measuring the reflection of a laser beam pointed at a surface. Methane will adsorb part of the beam, and this adsorption changes the reflected beam, which allows a methane measurement in the air to be made. The laser reading is dependent upon the distance that the laser beam travels through a gas cloud containing methane. Therefore, the units of data collected from laser methane detectors are always per unit of distance, e.g. metre, for example ppm/m, %Volume/m or %LEL/m. Data readings are most often presented in ppm/m, which changes due to length of the plume (Figure 51). For example, a ppm/m reading of 50 ppm can be indicative of a 1 m long methane plume (or “cloud”) with an internal methane concentration of 50 ppm/volume, or, alternatively it can be indicative of a 10 m long methane plume, with an internal methane concentration of 5 ppm/volume. As a result, the laser meter ppm/m readings will also change depending on the angle that the beam enters a plume; for example, if it is parallel to the plume length then it will be higher than if it is perpendicular to the plume length. Given this, laser methane data need to be interpreted in context, and generally are only effective at detecting possible methane plumes from point-sources following repeated stationary measurements at individual sites.

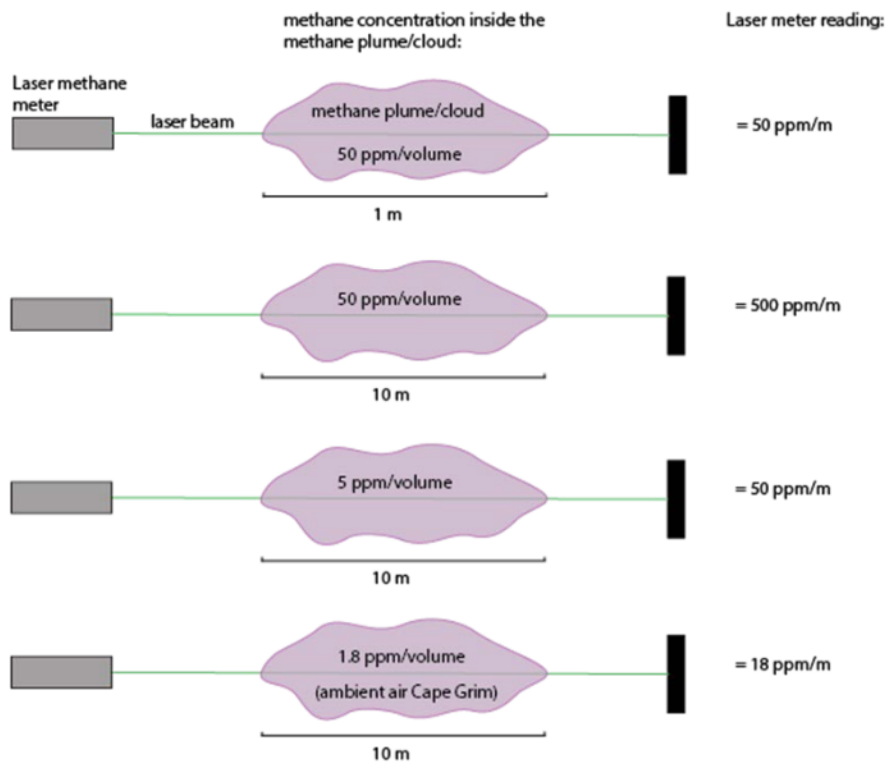


Figure 51: Conceptual representation of the effect of gas plume/cloud on raw laser methane meter data readings.

During a methane survey, a laser methane detector is used by pointing the laser beam at the ground surface and traversing a transect with the laser data continually logging. Readings below 25 ppm/m are generally considered within background limits, although higher readings (up to 500 ppm/m) may occur due to a number of factors not related to a point source methane leak, including: measurement error; dust or other interference; and the presence of multiple or diffuse sources of methane nearby. For this survey, when readings along the seismic anomaly transect were detected > 100 ppm/m, the vehicle was stopped and repeated measurements were made around the area from different angles where a high reading was detected. Under a scenario where a point-source of methane discharge was occurring, a plume of methane would be detected by the laser methane detector: this would be confirmed by repeated, stationary high ppm/m readings at the site. If repeated, stationary measurements could not be confirmed it would be concluded that a point-source plume of methane does not exist at that site.

Methane flux data collection

The gas flow rate was measured using an Eagle 2 gas monitor and static flux-hood according to the requirements outlined in the AS/NZS 4323.3:2009 Australian/New Zealand Standard. Stationary source emissions. Method 4: Area source sampling — Flux chamber technique. The gas flow rate was calculated according to the requirements outlined in Appendix C, Guidance on monitoring landfill gas surface emissions, LFTGN07, UK Environment Agency, 2010. The gas quantity at the site has been evaluated using the gas flux emissions calculated using the following equation:

$$Q = V \times (dc/dt) A$$

Where:

Q is the gas flow rate (mg/m²/s);

V (m³) is the volume of the flux-hood used for the measurement;

A (m²) is the surface area of the flux-hood used for the measurement;

dc/dt = gradient of graph of methane concentration (mg/m³) versus time (seconds);

The rate of change of the gas concentration (dc/dt) is determined by plotting the data on charts with the x-axis representing time (in seconds) and the y-axis representing the mass concentrations (in % methane Low Explosion Limit (LEL)).

Gas composition data collection (summa canisters)

To determine the gas composition and concentration from data collected using summa canisters, samples were collected in accordance with USEPA method TO-15A, Determination of Volatile Organic Compounds (VOCs) in Ambient Air Using Specially Prepared Canisters with Subsequent Analysis by Gas Chromatography. Laboratory certified summa canisters (6L) were fitted with flow reducers to allow sampling over 24 hours. The samples were analysed by a National Association of Testing Authority Australia (NATA) accredited laboratory for:

- Permanent gases (CO, CO₂, O₂, and H₂); and
- Methane and light hydrocarbons (ethane, ethene, propane and butane).

The summa canisters were deployed at three locations for 24 hours:

- 1) At abandoned coal hole R2315 using flux hoods to determine the composition of soil gases fluxing towards the atmosphere at:
 - i. The ground surface immediately adjacent to the plugged R2315 coalhole
 - ii. The ground surface ~ 10 m from the plugged R2315 coalhole
- 2) At an unidentified open coalhole on Greenswamp Road – here referred to as Hole 1 to determine free gas composition:
 - i. of gas at the opening of Hole 1 (by inserting a tube connected to the summa canister into the opening of Hole 1); and
 - ii. of atmospheric gases ~ 10 m from Hole 1
- 3) Atmospheric gases at Chinchilla (field blanks)

The locations and samples description have been summarised in Table 10 below.

	Sample ID	GS001	GS002	GS003	GS004	GS005	GS006	GS007	GS008
Location description		R2315*	R2315*	R2315*	R2315*	Hole 1*	Hole 1*	Chinchilla	Chinchilla
Samples description		Ground with flux hood at R2315	Ambient air	Ground with flux hood, located at approximately 10 m away	Ambient air, located at approximately 10 m away	Inside hole	Ambient air	Blank	Blank
Compounds	LOR (Mol %)	(Mol %)	(Mol %)	(Mol %)	(Mol %)	(Mol %)	(Mol %)	(Mol %)	(Mol %)
Light Hydrocarbons									
Methane	0.050	<0.100	<0.100	<0.125	<0.100	<0.100	<0.100	----	----
Ethane	0.010	<0.020	<0.020	<0.025	<0.020	<0.020	<0.020	----	----

	Sample ID	GS001	GS002	GS003	GS004	GS005	GS006	GS007	GS008
Location description		R2315*	R2315*	R2315*	R2315*	Hole 1*	Hole 1*	Chinchilla	Chinchilla
Samples description		Ground with flux hood at R2315	Ambient air	Ground with flux hood, located at approximately 10 m away	Ambient air, located at approximately 10 m away	Inside hole	Ambient air	Blank	Blank
Compounds	LOR (Mol %)	(Mol %)	(Mol %)	(Mol %)	(Mol %)	(Mol %)	(Mol %)	(Mol %)	(Mol %)
Ethene	0.010	<0.020	<0.020	<0.025	<0.020	<0.020	<0.020	----	----
Propane	0.010	<0.020	<0.020	<0.025	<0.020	<0.020	<0.020	----	----
Butane	0.05	<0.10	<0.10	<0.12	<0.10	<0.10	<0.10	----	----
Permanent Gases	LOR (Mol %)	(Mol %)	(Mol %)	(Mol %)	(Mol %)	(Mol %)	(Mol %)	(Mol %)	(Mol %)
Carbon Dioxide	0.005	0.903	0.028	0.028	0.029	0.048	0.027	0.030	0.037
Carbon Monoxide	0.0005	<0.0010	<0.0010	<0.0012	<0.0010	<0.0010	<0.0010	<0.0010	<0.0010
Hydrogen	0.005	<0.010	<0.010	<0.012	<0.010	<0.010	<0.010	<0.010	<0.010
Helium	0.005	<0.010	<0.010	<0.012	<0.010	<0.010	<0.010	<0.010	<0.010
Oxygen	0.10	17.7	19.8	21.0	20.1	20.5	19.7	19.9	19.6
Inert Gases (N2, Ar) by difference	0.10	81.4	80.2	79.0	79.9	79.5	80.3	80.1	80.4

Table 10: Analytical gas composition results from summa canisters (*R2315: -26.804045, 150.467084), *Hole 1 (-26.778158, 150.530634).

Results of laser methane detector data surveys are shown in Figure 52 and Figure 53. Two locations with high readings (>500 ppm/m) were detected during the survey:

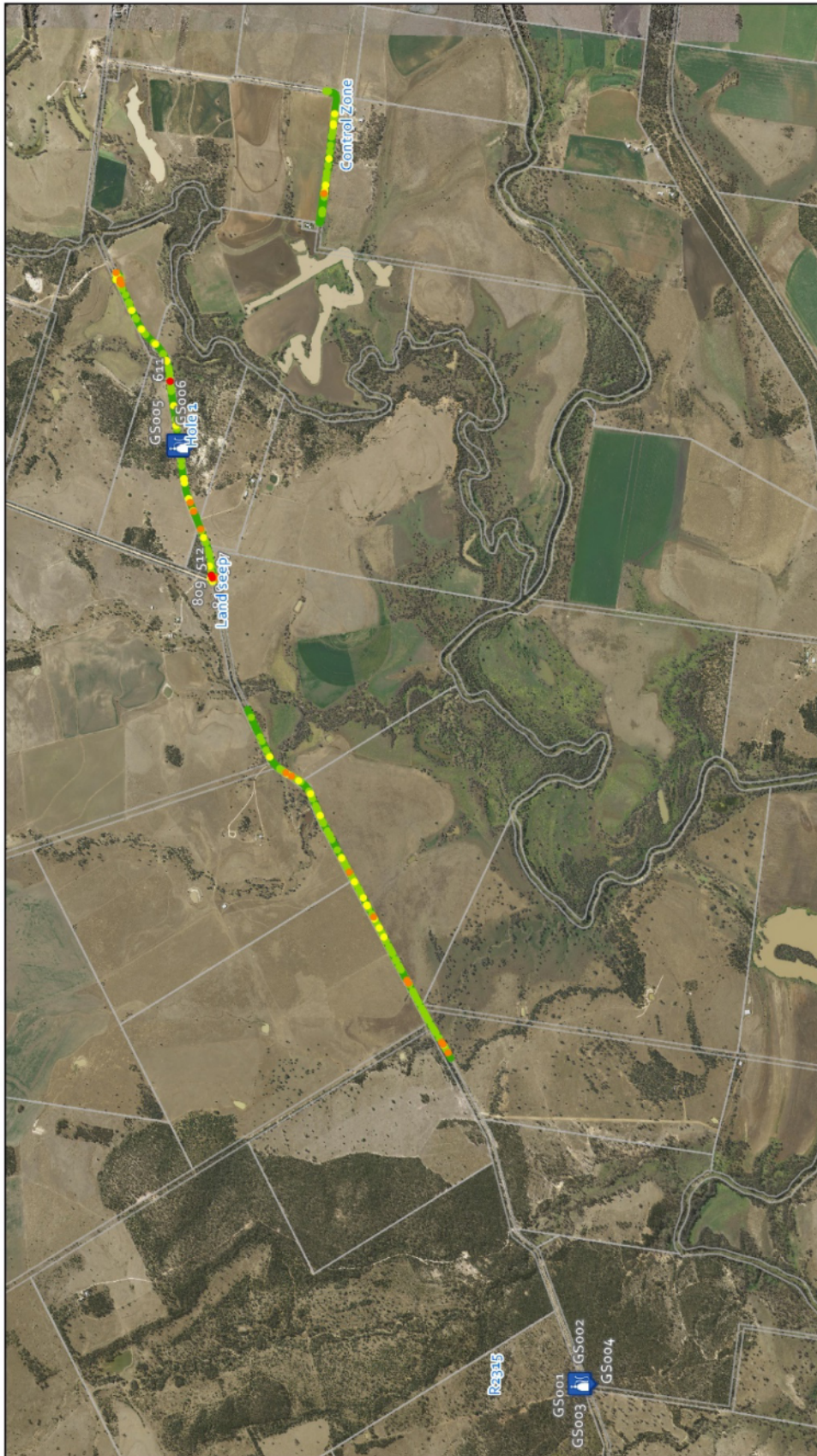
- The atmospheric headspace of the unnamed coalhole (Hole 1) – 611 ppm/m
- Methane discharges from the land surface at the road verge at the intersection of Greenswamp Road and Baking Board Road – 512 ppm/m to 1281 ppm/m.

The high reading (611 ppm/m) at Hole 1 is indicative of methane flux from this coal hole. However, summa canister results for this site did not detect high methane or other hydrocarbon compositions of atmospheric air (Table 10): this may be because any methane discharging from the coalhole rapidly dissipates, and dilutes in the atmosphere near the hole opening.

The high methane ppm/m readings from the land surface at the corner of Greenswamp and Baking Board Road likely reflects a buried coalhole, although this was not confirmed during this study. An example of soil methane fluxes from this site (Latitude: -26.780070, Longitude: 150.522430) was calculated using flux hood data, being 43.9 ppm/s (0.00439 Mol%/s, or 0.08% LEL/s).

The vehicle survey did not traverse the area of Greenswamp Road where coalhole R2315 occurs.


However, stationary laser methane readings were taken at this site, including around the abandoned coalhole and at an area ~10 m from the coalhole (where the summa canister was placed); although not logged georeferenced, these readings at this site were ~25 ppm/m or less, which is indicative of low methane headspace conditions, similar to ambient air. Gas composition from summa canister analyses showed that methane and other hydrocarbons were not above detection limit at this site, which provide further evidence of the absence of subsurface methane fluxes to the atmosphere at the site following abandonment, including immediately adjacent to R2315 and at a distance of ~10 m from the site.



 TERRA SANA CONSULTANTS	
 Summa Canister Locations	<p>Note: For legibility only concentrations above 500 ppm are labelled on the map.</p>
Legend	<p>Scale : 35,000 @A4</p>
<ul style="list-style-type: none"> ● Under 25 ppm ● Between 25 and 100 ppm ● Between 100 and 250 ppm ● Between 250 and 500 ppm ● Over 500 ppm 	<p>Coordinate System: GDA_94 Drawn by: Marc Dougherty Date: 26/02/2019</p>
 	<p>Map Credits: ESRI Data Source: Terra Sana C.</p>

Figure 52: Greenswamp Road – Surface methane gas monitoring walk-over and drive survey.





**TERRA SANA
CONSULTANTS**

Note: For legibility only concentrations above 500 ppm are labelled on the map.

Map Credits: ESRI | Data Source: Terra Sana C.

Map Credits: ESRI | Data Source: Terra Sana C.

Legend

- Under 25 ppm
- Between 25 and 100 ppm
- Between 100 and 250 ppm
- Between 250 and 500 ppm
- Over 500 ppm

Scale : 500 @A4

Coordinate System: GDA_94

Drawn by: Marc Dougherty

Date: 26/02/2019

Scale

0 5 10 20
Meters

Figure 53: Greenswamp Road – Surface methane gas monitoring walk-over survey.

8.3 Water well RN 17414 (Arrow Energy)

Renviro Pty Ltd is planning to commence a third field trial using a combined bentonite/grout design to abandon a water well for Arrow Energy Pty Ltd (registered bore number, RN – 17414). The bore is reported to be in poor conditions and no longer in use. The abandonment operations will start after the official end of the AQIP project.

9 Grant applications for future development

- **Cooperative Research Centre Projects (CRC-P)**
We applied for a CRC-P funding twice (Rounds 5 and 6). The first application was lodged by WGP Constructions Pty Ltd with the two partner organizations Nautic Australia Pty Ltd and The University of Queensland. The first proposal was unsuccessful because of insufficient cash contribution from The University of Queensland, but the partners were invited to reapply after solving this issue. This was done within the second application for Round 6. Unfortunately it was unsuccessful again, because it was assessed as “insufficiently competitive”.
- **Accelerating Commercialisation Program**
Renviro Pty Ltd in conjunction with UQ CCSG, is submitting a funding application to the Accelerating Commercialisation Federal program. This proposal is focused on commercialisation of Bentonite Plugs. This submission will be finalized by mid-April 2019, with evaluation and feedback from the Evaluation Committee a month after the Federal Government comes out of caretaker mode, which is expected to be July or August 2019. Renviro Pty Ltd has already submitted an Expression of Interest to participate in the Accelerating Commercialisation process and has been accepted to submit an official funding application.

10 Conclusions and outlook

The commercially available sources for bentonite in Queensland were identified and samples of raw material were taken to run an extensive laboratory program to detect physical and chemical properties of the raw material. We contacted the two biggest bentonite producers in Queensland (Sibelco Australia Pty Ltd and Amcol Australia Pty Ltd) to purchase raw sodium bentonite material for our laboratory experiments and for the production of bentonite plugs used in field trials. Only Amcol Australia Pty Ltd supported the project by providing three different raw bentonite materials mined in their Queensland Bentonite Mine.

The provided bentonites were analyzed to determine the mineralogical composition, chemistry of the raw bentonite, swelling performance and mechanical properties. We identified the 5D bentonite from Amcol Australia Pty Ltd as best performing material for the later abandonment field trials. QA/QC of the bentonite used for the plug production was necessary to ensure that the quality of the used material does not vary over different bulker bags/batches. The Queensland Bentonite Mine operated by Amcol Australia Pty Ltd reported a total historical production of 193.000t and total resources of 12Mt (von Gnielinski 2017). They are producing a high swelling sodium bentonite through a 80.000tpa processing plant located on the mine site. The supply of 5D bentonite is secured for years to come if the decision will be made to commercialize the bentonite technology and start mass production of

plugs.

Different failure modes depending on flow rates were identified during the hydraulic testing of the plugs using the Well Simulator Facility in the School of Chemical Engineering at UQ.

Frictional failure happens at the interface of the casing wall and bentonite plug and the entire plug is pushed out of the pipe. This happens only at high flow rates (Figure 27). Hydrated bentonite behaves like a non-Newtonian Fluid while failing (shear-thickening). A rapid pressure increase will trigger shear failure at the complete circumference of the plug at a high failure pressure. This could be very valuable in case of casing failure events.

Slow pumping creates single micro channels at the interface of the plug/steel pipe at much lower applied pressures (Figure 29 & Figure 30). At low flow rates failure modes are more complex and material/hydration time dependent. The 5D bentonite hydrates more quickly than the 5A and 5B materials. The hole in the center of the plugs is sealed earlier when using the 5D material compared with the two other candidates (see Figure 29 & Figure 30).

The identification of the micro channeling effect impacts the design for well abandonment planning. The lower failure pressure levels for gas compared to water detected in this study have to be taken into account for the abandonment planning of different well types. Failure pressures are roughly 50% higher for the bentonite/PVP blend plugs while using water than failure pressures using air. The failure gradients reported in Table 9 are based on failure using water as the pumping medium. They have to be corrected to 50% lower pressure gradients for free gas containing wells.

Nuclear magnetic resonance (NMR) experiments might help to create a better understanding of the process of the micro channeling generation. A future project should use this or an alternative suitable detection technique to try to map/visualize the growth of these channels at the interface of the plug/steel pipe during a hydraulic test.

The reported results of this study allow detailed abandonment planning of different well types. This technology is suitable to be used securely for open hole or fully cased water, water monitoring, CSG wells and coal exploration wells. A water monitoring well in an active CSG field and a coal exploration well are already successfully abandoned (Chapter 8) and a third field trial is planned to be commenced in the near future.

Major lessons learned from these field trials are documented in Chapter 8 and associated appendices. These are mostly dealing with optimization of operational sequences concerning the plug placement. Using spacers to pump plugs out of the pipe used for placement simplifies the deployment process. We would have been able to place all the plugs within one day, if we have had enough of these spacers available on the R2315 rig site.

We also learned how coalbores drilled in the 1980s used to be abandoned. Appendix 16 gives an overview of the R2315 plugging and abandonment (P&A) operations. We found a fence post while drilling the top hole to set a conductor casing. Other wells abandoned at this time may have been abandoned in a similar manner. If so, these wells are technically not abandoned and are emitting changing volumes of methane, depending on their free water level.

Commercialisation of this technology is the next step. It is necessary to scale up the production by designing a commercial size plug table press, which is able to deliver multiple plugs with one stroke.

The more important future development has to be the design of a rig-less abandonment technology, because this will create major saving potential for the operators. Two applications for CRC-P funding (Chapter 9) to develop the crucially needed technology were unsuccessful. Renviro Pty Ltd in partnership with UQ CCSG is now preparing an application for alternate federal funding for the commercialisation process. The proposal for the Accelerating Commercialisation Program will be submitted by mid-April 2019 but a result of the evaluation is not expected to be available before Q3 2019.

11 References

- Anderson, L., Bai, Y., Huseeth, K. & Melton, M. (2013): Simulation of Wellbore Plugging with Bentonite. - May 2013. University of Wyoming Department of Chemical and Petroleum Engineering, Unpublished Senior Design report.
- Baublys, K. A., Hamilton, S. K., Golding, S. D., Vink, S. & Esterle, J. (2015): Microbial controls on the origin and evolution of coal seam gases and production waters of the Walloon Subgroup; Surat Basin, Australia. - *International Journal of Coal Geology*, 147–148, 85-104.
- Bell, S. R., Opitz, L.A., Sundstrom, E. & Taylor J.F. (2009): Plugging Wells with Hydrated Bentonite, Lab Results. - May 2009. University of Wyoming Department of Chemical and Petroleum Engineering, Unpublished Senior Design report.
- Blach, T. & Holl, H.-G. (2018): Small Angle Neutron Scattering investigation of compressed Bentonite. – Internal report, Centre for Coal Seam Gas, University of Queensland.
- Bucher, F. & Müller-VonMoos, M. (1989): Bentonite as a containment barrier for the disposal of highly radioactive waste. - *Applied Clay Science*, 4(2): 157–177.
- Carlson, L. (2004): Bentonite Mineralogy – Part 2: Mineralogical Research of Selected Bentonites. – POSIVA Working Report, **2004-02**.
- Clark, J. & Salsbury, B. (2003): Well Abandonment Using Highly Compressed Sodium Bentonite, An Australian Case Study. - SPE 80592, SPE/EPA/DOE Exploration and Production Environmental Conference held in San Antonio, Texas, U.S.A., 10-12 March 2003.
- Draper, J. J. & Boreham, C. J. (2006): Geological controls on exploitable coal seam gas distribution in Queensland. - *APPEA Journal*, 46, 343–366.
- Englehardt, J., Wilson, M.J. & Woody, F. (2001): New Abandonment Technology New Materials and Placement Techniques. - SPE 66496, SPE/EPA/DOE Exploration and Production Environmental Conference held in San Antonio, Texas, 26-28 February 2001.
- Golding, S. D., Boreham, C. J. & Esterle, J. S. (2013): Stable isotope geochemistry of coal bed and shale gas and related production waters: A review. - *International Journal of Coal Geology*, 120, 24-40.
- Hamilton, S. K., Golding, S. D., Baublys, K. A. & Esterle, J. S. (2014): Stable isotopic and molecular composition of desorbed coal seam gases from the Walloon Subgroup, Eastern Surat Basin, Australia. - *International Journal of Coal Geology*, 122, 21-36.
- Holl, H.-G. (2016a): Bentonite project – Baseline data study and recommended future work. - Internal report, Centre for Coal Seam Gas, University of Queensland.
- Holl, H.-G. (2016b): Mine visit at the Minerals Technologies, Amcol Australia Pty Ltd Queensland Bentonite Mine (17th of February, 2016). Internal File Note, Centre for Coal Seam Gas, University of Queensland.
- Holl, H.G. & Scheuermann, A. (2018): Characterisation of Geomechanical Properties of Bentonite Clay

Used for Plug and Abandonment Operations of Coal Seam Gas Wells. – Journal of Minerals and Materials Characterization and engineering, **6**, 218-234; <https://doi.org/10.4236/jmmce.2018.62016>.

Koelling, E., Haakinson, D. & Esquivel D. (2011): Bentonite Properties. - May 2011, University of Wyoming Department of Chemical and Petroleum Engineering, Unpublished Senior Design report.

Moore, D.M. & Reynolds, R.C., Jr. (1997): X-Ray Diffraction and the Identification and Analysis of Clay Minerals – 2nd edition. – Oxford United Press.

Mortezapour A. (2016): Laboratory Testing of Queensland Bentonite. - MPhil University of Queensland, School of Chemical Engineering, September 2016.

Muurinen, A. (2011): Measurements of Cation Exchange Capacity of Bentonite in the Long-Term Test of Buffer Material (LOT). – POSIVA Working Report, 2011-10.

Oueslati, W., Ben Raheim, H., Lanson, B. & Ben Haj Amara, A. (2009): Selectivity of Na-montmorillonite in relation with the concentration of bivalent cation (Cu^{2+} , Ca^{2+} , Ni^{2+}) by quantitative analysis of XRD patterns. – Applied Clay Science, **43**, 224-227.

Owen, D. D. R., Shouakar-Stash, O., Morgenstern, U. & Aravena, R. (2016): Thermodynamic and hydrochemical controls on CH₄ in a coal seam gas and overlying alluvial aquifer: new insights into CH₄ origins. - Scientific Reports, **6**, 32407.

Rayment, G.E. & Lyons, D.J. (2011): Soil Chemical Methods – Australasia. Published as ePDF by CSIRO Publishing.

Raftery, T. (2018): QUT Central Analytical Research Facility – Materials Characterisation Report.

Rengasamy, P. & Churchman, G.J. (1999): Cation Exchange Capacity, Exchangeable Cations and Sodicity. In: [Soil Analysis: an Interpretation Manual](#). (Eds: Peverill, K.I., Sparrow, L.A. and Reuter, D.J.) – CSIRO Publishing.

Scheuermann, A. & Holl, H.-G. (2017): Mechanical Properties of Bentonite Plugs. – Internal report, Centre for Coal Seam Gas, University of Queensland.

Scoggings, A. (2014): AMCOL Australia's Gurulmundi mine. A leading supplier of high quality sodium bentonites. – Industrial Minerals, June 2014, 39-43.

Spratt, H. & Raftery, T. (2016a): Powder X-Ray Diffraction Analysis of Submitted Samples (2T, 2M, 2B to 8T, 8M, 8B and CL).

Spratt, H. & Raftery, T. (2016b): Powder X-Ray Diffraction Analysis of Submitted Samples – Clay Results.

Stalker, L. (2013): Methane Origins and behaviour. – Report to the Office of the NSW Chief Scientist and Engineer, CSIRO, Australia.

Towler, B. F. & Ehlers, G. C. (1997): Plugging Wells with Hydrated Bentonite, Part 1: Friction Factors - SPE 38347, SPE Rocky Mountain Regional Meeting, Casper, WY, May 18-21, 1997.

Towler, B. F., Victorov, H., Zamfir, G. & Ignat, P. (2008): Plugging Wells with Hydrated Bentonite, Part 2: Bentonite Bars. - SPE 115524, SPE Annual Technical and Exhibition, Denver CO, 21–24 September

2008.

Towler, B.F., Firouzi, M., Morteza pour, A. and Hywel-Evans, P.D. (2015): Plugging CSG Wells with Bentonite: Review and Preliminary Lab Results. – SPE-176987-MS, SPE Asia Pacific Unconventional Resources Conference, Brisbane, Australia, 9-11th Nov. 2015.

Towler, B., Firouzi, M. and Hywel-Evans, P.D. (in prep): Failure modes for hydrated bentonite plugs when used in well decommissioning operations.

von Gnielinski, F.E., (Compiler) (2017): Queensland Minerals 2016, a summary of major mineral resources, mines and projects. Department of Natural Resources and Mines, Queensland.

12 Appendices

The appendices can be downloaded from: <https://cloudstor.aarnet.edu.au/plus/s/ITW4rR1J17JaMAI>

Appendix 01: QUT Central Analytical Research Facility – Materials Characterisation Report.

Appendix 02: Powder X-Ray Diffraction Analysis of Submitted Samples (2T, 2M, 2B to 8T, 8M, 8B and CL).

Appendix 03: Powder X-Ray Diffraction Analysis of Submitted Samples – Clay Results.

Appendix 04: File Note – Mine visit at the Minerals Technologies, Amcol Australia Pty Ltd Queensland Bentonite Mine (17th of February, 2016).

Appendix 05: Bentonite project – Baseline data study and recommended future work.

Appendix 06: Material specifications sheets of bentonite providers.

Appendix 07: Mechanical Properties of Bentonite Plugs.

Appendix 08: Small Angle Neutron Scattering investigation of compressed Bentonite.

Appendix 09: Failure modes for hydrated bentonite plugs when used in well decommissioning operations.

Appendix 10: Bentonite Plug Dislodgement Testing.

Appendix 11: Technical data sheet NaX™ WP 19 shrinking compensated grout.

Appendix 12: Technical data sheet CETCO® TABLETS, Bentonite tablets 0.25”.

Appendix 13: Overview Bellevue #GW3 abandonment operations.

Appendix 14: Operations summary report Bellevue #GW3.

Appendix 15: P&A report R2315.

Appendix 16: Overview R2315 abandonment operations.

Appendix 17: UQ-CCSG Research Review 2018, Poster Holl.

Appendix 18: Bore 2315 Gas Readings Report Draft, DNRME.